

Proposal for a Hadron Blind Detector for PHENIX

Z. Fraenkel, B. Khachaturov, A. Kozlov, A. Milov,
D. Mukhopadhyay, D. Pal, I. Ravinovich,
I. Tserruya and S. Zhou

Weizmann Institute of Science, Rehovot

June 2001

Abstract

This note discusses the possibility to measure low-mass e^+e^- pairs ($m_{e^+e^-} \leq 1\text{GeV}/c^2$ including the light vector mesons ρ, ω and ϕ , and the low-mass continuum) using an HBD (Hadron Blind Detector) located at $R=20\text{-}60\text{cm}$. It has two main parts: the first part deals with Monte Carlo studies. The discussion is kept most of the time at the principle level, using idealistic assumptions to unveil the physics limitations. It starts with a description of the assumptions and procedures used all along the study, briefly reviews the present capabilities of the PHENIX baseline detector and then focusses on an upgrade concept which dramatically improves the performance and leads to a definition of the system specifications. The second part considers a possible realization of the upgrade scheme. Various options for the key elements (gases, detector configuration and readout chambers) and their basic properties are discussed in detail. The choice that emerges is a windowless Cherenkov detector, operated with pure CF_4 in a special proximity focus configuration, with GEM readout. A number of questions and issues are uncertain or require confirmation and those form the basis of a comprehensive R&D programme which is outlined at the end of this note.

PART ONE: MONTE CARLO STUDIES ¹

1. PROCEDURE AND INPUT PARAMETERS

This section gives details about the procedure used, the event generation (based on HIJING), the e^+e^- signal ($\phi \rightarrow e^+e^-$) and the electron background sources (from π^0 Dalitz decays and γ conversions).

1.1. Primary particles.

The study is performed for central Au-Au collisions at $\sqrt{s_{NN}} = 200$ GeV. The primary particles are only π^+ , π^- and π^0 with the following assumptions:

- $N_{\pi^+} = N_{\pi^-} = N_{\pi^0} = 3000$ in full space
- $\implies \left(\frac{dN}{dy}\right)_{y=0} = 475\pi^+ = 475\pi^- = 475\pi^0$
- p_T and y distributions are taken from HIJING.

We are using an “ideal tracking” scheme of the charged particles in the magnetic field using a look-up table. Here “ideal” means that multiple scattering and other physical processes are neglected. However the momentum is smeared according to the following resolution:

$$\frac{\sigma_p}{p} = 0.005 * \sqrt{1 + p^2} \quad \text{where } p \text{ is in GeV.} \quad (1)$$

All throughout this document a **track** is defined as a charged particle with $p_T > 200$ MeV going through PC1 and PC3. This follows from the assumption that it will not be possible in PHENIX to track particles with $p_T < 200$ MeV. With these definitions and assumptions, we have a total of 208 tracks per event (from π^\pm) in the acceptance of the two central arms, see Table 1. Fig. 1 shows the central arm track acceptance for pions in y and ϕ , with its well known peculiarities at low-momenta, in particular the “side feeding” of particles curved into the fiducial acceptance.

1.2. Signal: acceptance and rate

For the e^+e^- **signal** we consider, as a representative example, the ϕ -meson decay:

$$\phi \rightarrow e^+e^-$$

using the “rv_phi” generator. Fig. 2 shows the momentum and opening angle distributions of the electrons (right panels) within the central arm acceptance and with the p_T cut of 200 MeV. The rapidity and momentum distributions of the corresponding ϕ mesons are also shown in the same figure (left panels).

The ϕ -meson production rate is defined with respect to the π^0 yield as:

$$N_\phi/N_{\pi^0} = 0.015 \quad (2)$$

¹This part is largely based on work done by W.Xie while he was at the Weizmann Institute.

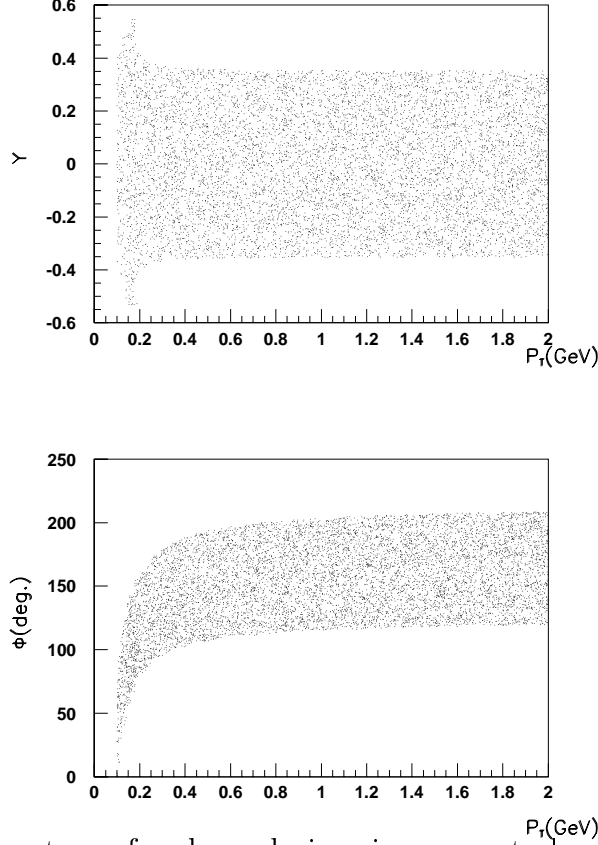


Figure 1. PHENIX acceptance for charged pions in one central arm.

The ϕ -meson density at mid-rapidity is 16% of all ϕ -mesons produced:

$$\frac{(dN_\phi/dy)|_{|y|<0.5}}{N_\phi} = 16\% \quad (3)$$

The acceptance of ϕ -meson decays, $\phi \rightarrow e^+e^-$, in the two central arms, taking into account the p_T cut of 200 MeV, is:

$$\frac{N_{\phi \rightarrow e^+e^-}(acc., p_t > 200)}{(dN_\phi/dy)|_{|y|<0.5}} = 2.9\% * BR \quad (4)$$

where $BR = 3 * 10^{-4}$ is the branching ratio of the $\phi \rightarrow e^+e^-$ decay². Note that the probability to detect a ϕ -meson in one single arm is negligibly small.

From the numbers quoted above, one can deduce the ϕ -meson production rate in PHENIX:

$$\begin{aligned} N_{\phi \rightarrow e^+e^-}(acc., p_t > 200) &= 0.015 * 0.16 * 0.029 * 3 * 10^{-4} * N_{\pi^0} \\ &= 2.1 * 10^{-8} * N_{\pi^0} \\ &= 6.2 * 10^{-5} \phi/event \end{aligned} \quad (5)$$

²The pair acceptance increases from 2.9% to 3.3% in the upgraded configuration that will be discussed later due to the reduction of the magnetic field.

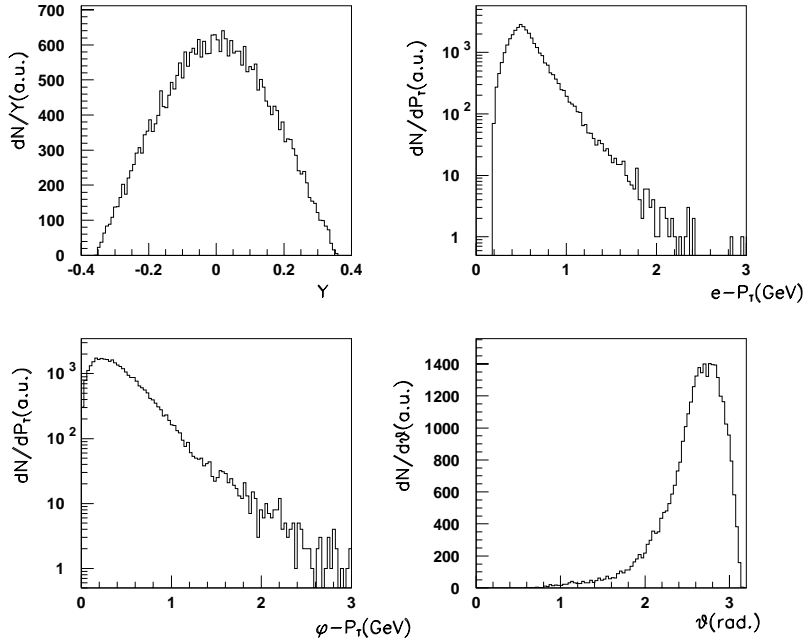


Figure 2. $\phi \rightarrow e^+e^-$ acceptance in the two central arms.

1.3. Background Sources

In the present study we have considered that the electron **background** originates from two sources ³:

- π^0 Dalitz decay, produced using standard PISA routines.
- γ conversions assuming a total radiation length $X/X_0 = 1\%$ (representing the estimated material budget from the beam pipe and MVD). The conversions are generated using standard routines from GEANT 3.21 and for simplicity, all conversions are generated at the vertex.

Each source contributes almost the same amount of background electrons and together they produce a total of 1.26 electron tracks per event, see Table 1. Most of these tracks, 1.13 track/evt, are *single electron tracks*, i.e. the partner cannot be recognized because it has a low momentum ($p_T < 200$ MeV) or is outside the fiducial acceptance. Approximately 10% of them, 0.13 track/evt, are from pairs where both tracks are in the acceptance. These can potentially be fully reconstructed and their contribution to the combinatorial background can be eliminated by applying a mass cut (see below).

1.4. Summary of track acceptance

The numbers quoted above for the signal, e^\pm background tracks, and π^\pm charged tracks per event within the acceptance of the two central arms in the present PHENIX configuration are summarized in Table 1. Again the counting is done for tracks with $p_T > 200$ MeV

³These are certainly the dominant sources. However, at RHIC energies, open charm might be a significant source of single electrons and we plan to include its contribution in more refined studies.

going through PC1 and PC3.

Table 1

Number of e^\pm background tracks, π^\pm charged tracks and signal pair per event in the present PHENIX configuration

		singles	pairs
<u>Signal</u>	$\phi \rightarrow e^+e^-$		$6.2 \times 10^{-5} \phi/evt$
<u>Background</u>	$\pi^0 \rightarrow e^+e^-\gamma$	0.51	0.06
	$\gamma \rightarrow e^+e^-$	0.62	0.07
	Total electrons	1.13 tr/evt	0.13 tr/evt
<u>Charged tracks π^\pm</u>		208 tr/evt	

2. PERFORMANCE OF PRESENT PHENIX CONFIGURATION: COMBINATORIAL e^+e^- MASS SPECTRUM AND S/B RATIO

Based on the track acceptance calculations and particle production rates, one can calculate the combinatorial background mass spectrum. We again use ideal conditions, i.e. assuming infinite pion rejection and 100% electron efficiency. Furthermore, all electron tracks forming a pair with mass $m < 130 \text{ MeV}/c^2$ are removed and only the remaining electrons are paired with each other. This mass cut removes the pairs from π^0 Dalitz decays and γ conversions where both tracks are reconstructed and consequently, the combinatorial background is produced only by the *single* tracks (see Table 1). The resulting combinatorial mass spectra for ‘‘Like’’ and ‘‘Unlike’’ sign pairs and their difference are shown in Fig. 3.

In order to see the effect of the ideal assumptions, we also calculated the combinatorial background for finite π rejection. The results are shown in Fig. 4 for rejection factors of ∞ , 1000, 500 and 200. The figure shows the total combinatorial background (solid line) as well as the various individual contributions from electron-electron (dashed line), electron-pion (dotted line) and pion-pion (dashed-dotted line) combinations. For comparison the relative strength of the ϕ signal is also indicated in the figures. One sees that for a π rejection factor of 200 the combinatorial background increases by a factor of ~ 7 at the ϕ mass with respect to the ideal case of infinite pion rejection.

The performance can quantitatively be characterized by the signal to background (S/B) ratio at the ϕ mass. The yields of the signal and background are determined by integrating the corresponding mass spectra within $\pm 1.5\sigma$ around the ϕ mass peak, where $\sigma = 4.3 \text{ MeV}$

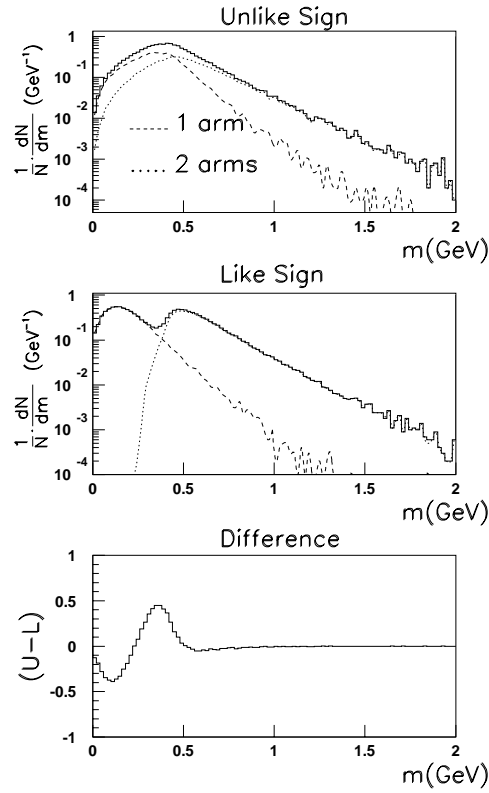


Figure 3. Combinatorial e^+e^- mass spectra for “like” and “unlike” sign pairs.

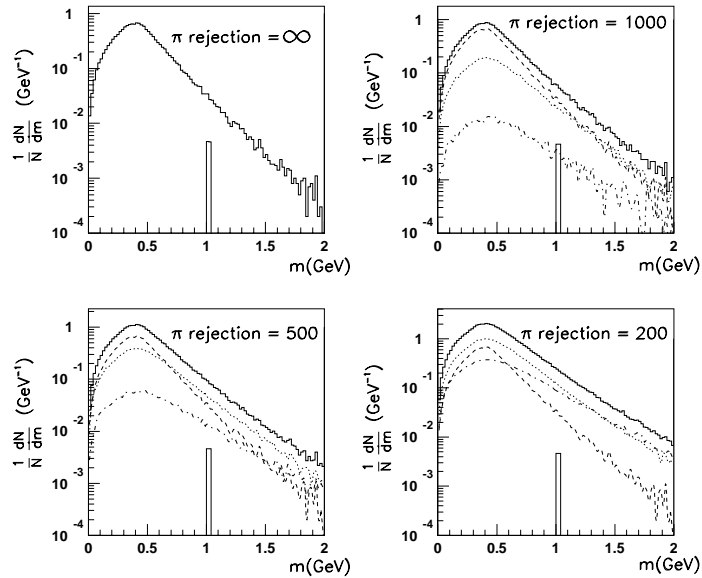


Figure 4. Combinatorial e^+e^- mass spectra for different π rejection factors in the present PHENIX configuration. Also shown are the individual contributions from electron-electron (dashed line), electron-pion (dotted line) and pion-pion (dashed-dotted line) combinations, as well as the relative strength of the ϕ signal.

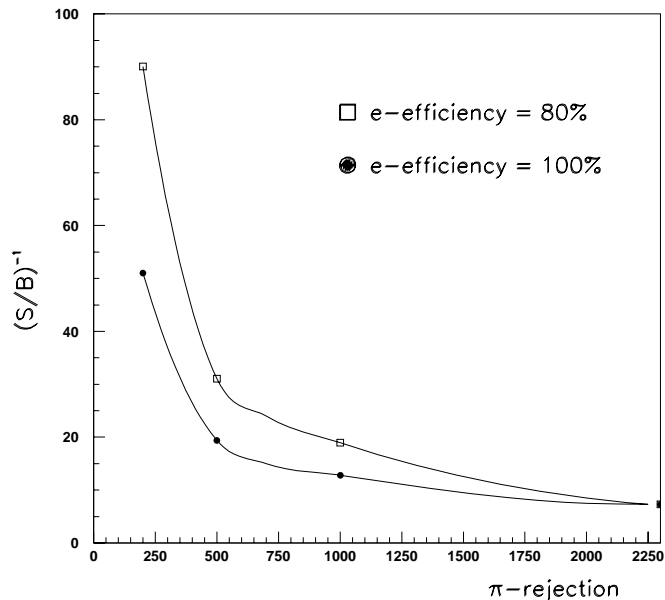


Figure 5. $(S/B)^{-1}$ as a function of the π rejection factor for 100 and 80% single electron track efficiency

is the expected mass resolution at the ϕ mass region. The results are presented in Table 2 and also plotted in Fig. 5 as solid symbols. These numbers are very close to those found by Akiba long time ago under more or less similar conditions.

Table 2

Signal to Background ratio, S/B for different π rejection factors

π rejection	(S/B)
inf.	1/7
1000	1/12
500	1/19
200	1/51

Finally, we illustrate the effect of relaxing the second ideal assumption of perfect electron identification, by repeating the calculations for a single electron detection efficiency of 80%. The results are shown in Fig. 5 as open symbols. With an electron track efficiency of 80% the signal rate drops to 64%. However, the S/B ratio is not affected too much. It only deteriorates by less than 10% as long as the π rejection is above 1000. This can be easily understood since to first order the electron efficiency affects equally the signal and the background. In other words, for the e^+e^- pair tracking, the π -rejection factor is the most critical factor as far as quality, i.e. S/B ratio, is concerned. We can tolerate a relatively low single electron track efficiency, the price to pay will be in the event rate and not so much in the quality of the results.

3. PERFORMANCE OF UPGRADED PHENIX CONFIGURATION

3.1. General Guidelines and Opening Angle Cut

In order to improve the situation, we need better recognition and thereby better rejection of electron tracks originating from π^0 Dalitz decays and γ conversions. We think that the best and most promising way is the upgrade concept that was already contemplated in the original PHENIX design: installation of a second coil to generate a field free region extending up to 60 cm in the radial direction and some additional detector in that region to provide the necessary rejection of Dalitz and conversion tracks. The basic idea is that in the field free region the pair opening angle is preserved, thus allowing us to exploit, by applying a close-hit cut, the fact that pairs originating from π^0 Dalitz decays and γ conversions have a very small opening angle compared to pairs from ϕ -meson decays. Fig. 6 shows the opening angle of the pairs of interest, π^0 Dalitz and γ conversions pairs with at least one track with $p_T > 200$ MeV and ϕ meson decays with both tracks having $p_T > 200$ MeV. With an opening angle cut of ~ 200 mrad one can reject $\sim 90\%$ of the conversions and π^0 Dalitz decays, while preserving most of the signal.

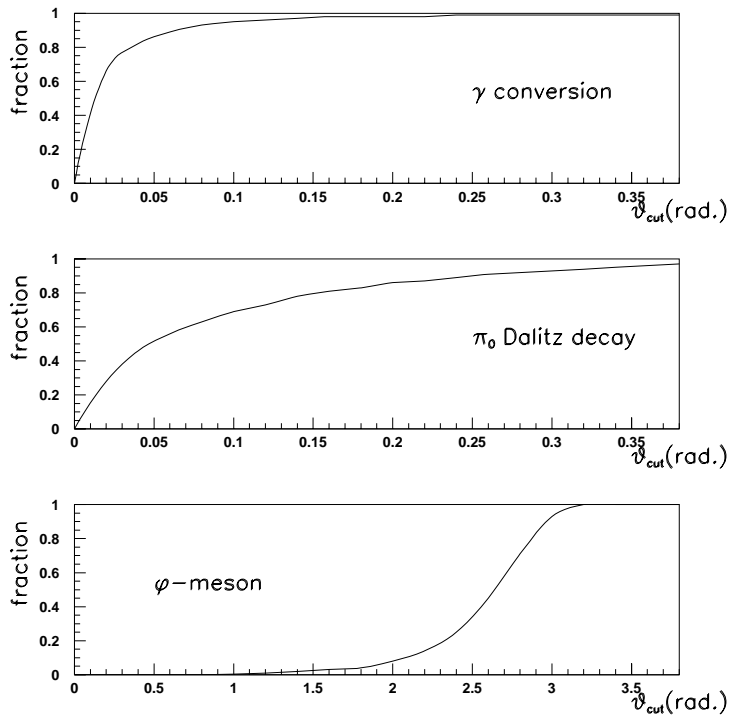


Figure 6. Integrated opening angle distributions. The figures show the fraction rejected by applying an opening angle cut as function of the opening angle cut.

Throughout the rest of this note we will assume that the zero field region extends to $R = 60$ cm and stays unchanged from its present strength above that radius. The specifications of the inner detector will be defined as we go along. The goal is to achieve,

under ideal simulations, a S/B ratio of $\sim 10/1$ i.e. two orders of magnitude better than the present configuration. Since the combinatorial background depends quadratically on the number of tracks, we must reject conversions and π^0 Dalitz decays at least to the 90% level thus implying a single electron efficiency of at least 90% in the inner detector.

3.2. Hits and Tracks in the Upgraded Configuration

The number of hits in the inner detector and tracks in the outer detectors (PC1 and PC3) originating from electrons and from charged particles are summarized in Table 3.

Table 3

Hits and tracks per event statistics in the Upgraded PHENIX Configuration

- **Hits in inner detector** (*no p_T cut*)

e^\pm hits:	$\pi^0 \rightarrow e^+e^-\gamma$	4.1
	$\gamma \rightarrow e^+e^-$	5.1
	Total	9.2 e-hits/evt
π^\pm hits:	280 π/evt = 173 tracks + 107 hits	

- **Tracks in outer detectors** ($p_T > 200$ MeV)

e^\pm tracks:

All:

0.20 pairs = 0.1 π^0 Dalitz + 0.1 γ conversions.

1.10 singles = 0.5 π^0 Dalitz + 0.6 γ conversions.

Mass cut ($m > 0.13$ GeV).

0.93 singles = 0.42 π^0 Dalitz + 0.51 γ conversions.

With a matched hit in inner detector.

0.70 singles = 0.32 π^0 Dalitz + 0.38 γ conversions.

π^\pm tracks: **208 π /evt**

- **ϕ Meson Signal**

Rate: $7.1 \cdot 10^{-5}$ per event	1.
Mass cut ($m > 0.13$ GeV).	0.92
With matched hits in inner detector.	0.76

- **S/B Ratio:**

Mass cut ($m > 0.13$ GeV)	S/B = 1/7
With matched hits in inner detector.	S/B = 1/5

The inner detector is sensitive to all particles emitted in the fiducial acceptance, without any p_T cut. There are 9.2 electrons + 280 charged pions per event, of which 173 can be tracked through the central arms (i.e. they have $p_T > 200$ MeV and they go through PC1 and PC3). In the present study we have not included additional hits, e.g. background hits originating from the magnet poles.

In the outer detectors (PC1 and PC3), the number of electron tracks per event is practically unchanged, (~ 1.1 single e-tracks per event before the mass cut and ~ 0.9 single e-tracks after the mass cut)⁴. The mere requirement that the outer electron track be matched to a hit in the inner detector brings already a reduction of the single electron track rate to 0.7 track/evt. The number of pions in the outer detectors is unchanged, 208 π /evt, of which as stated above, 173 have a matched hit in the inner detector and the remaining 35 probably originate from side feeding (see Fig. 1).

The rate of the ϕ meson signal has slightly increased from $6.2 \cdot 10^{-5}$ to $7.1 \cdot 10^{-5}$ due to the increased pair acceptance in the reduced field configuration. Throughout the rest of this note, we normalize this rate to 1 (i.e. the quoted signal rates have to be multiplied by $7.1 \cdot 10^{-5}$ to get the real signal rate). The mass cut reduces it to 0.92 and the requirement of matched hits in the inner detector for both tracks further reduces it to 0.76 ϕ /event.

The table also shows the S/B ratio. With the mass cut of 130 MeV/ c^2 , we obtain the same S/B ratio of 1/7 as obtained in the previous section. Requiring all electron tracks to be matched to a hit in the inner detector results in a small improvement to S/B = 1/5. This is due to the reduction of the signal (from 0.92 to 0.76) together with a stronger reduction of the background.

In the following we study in detail the benefits of the inner detector in improving the S/B ratio. We consider four different schemes:

- inner detector with perfect spatial resolution and no particle ID
- inner detector with perfect spatial resolution and perfect e identification
- same as 2 + veto area
- same as 3 with finite double hit resolution

3.3. Inner Detector with Perfect Spatial Resolution and no electron-id

This is the simplest option. The inner detector has no electron-id and the close hit cut is performed with all hits in the detector ($280\pi + 9e$). The results are shown in Fig. 7 left panels. The cut is very effective in reducing the background but at the same time it also kills the signal by random close hits in the inner detector. If we set as a guideline that we want to preserve $\sim 50\%$ of the signal then the close hit cut is limited to ~ 25 mrad

⁴We are neglecting the contribution of conversion electrons generated in the inner detector itself.

allowing an improvement of the S/B ratio to $S/B \sim 1$.

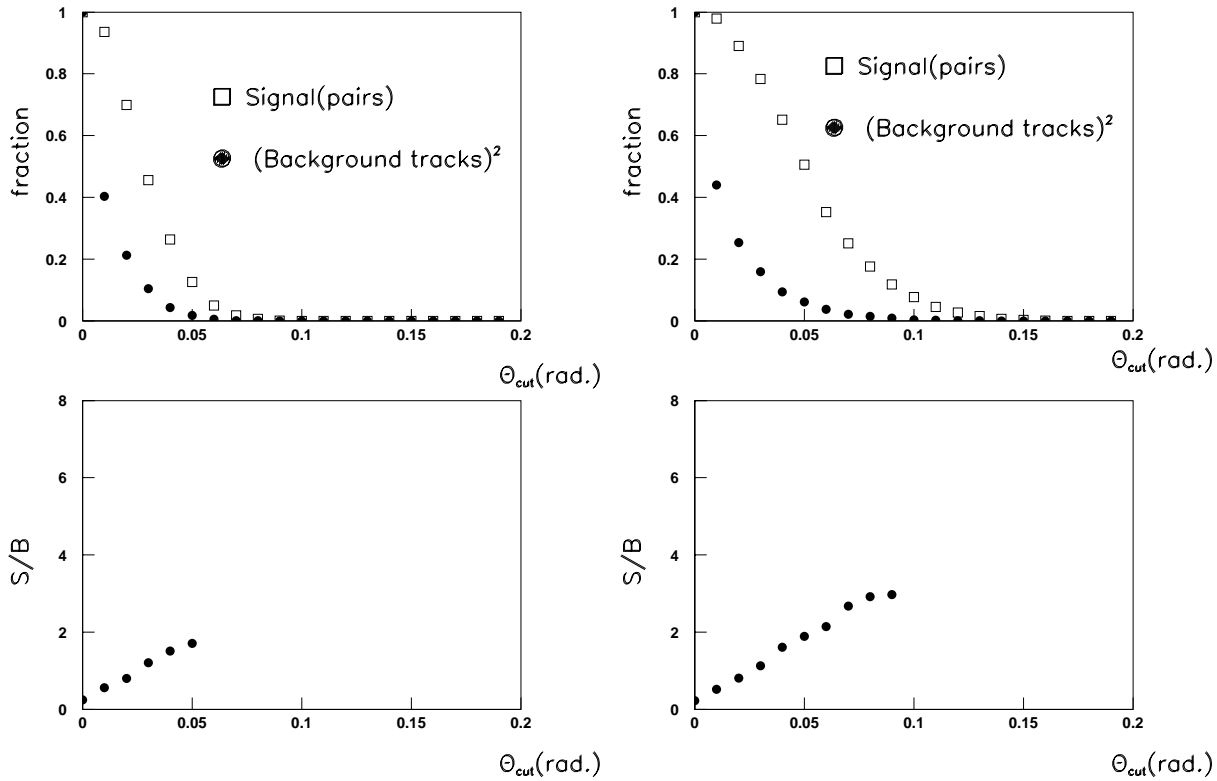


Figure 7. Signal, Background and S/B ratio without e-ID in the inner detector. Close hit cut performed with all $280\pi + 9e$ hits (left panels) and with only the $107\pi + 9e$ single hits (right panels)

We can somewhat improve the situation by limiting the close hit cut to single hits (as opposed to tracks) i.e. to the $107\pi + 9e$ which are not matched to the outer detectors. The results are shown on the right panels of Fig. 7. The close hit cut can now be extended to $\sim 50\text{mrad}$ allowing to reach a $S/B \sim 2$.

Conclusion: even the best detector in terms of spatial resolution but without electron-id will not allow us to reach the goal. The signal gets lost by random close hits in the inner detector.

3.4. Inner Detector with Perfect Spatial Resolution and Perfect electron-id

We assume now that the inner detector has perfect electron identification capability, so that the close hit cut is performed only with the 9 electron hits. The results are shown in Fig. 8. The left panel shows the absolute yield of ϕ mesons per event and of background

tracks per event (the contributions from γ conversions and π^0 Dalitz decays are shown separately) as a function of the opening angle cut θ_{cut} . The right panel shows the S/B ratio as a function of θ_{cut} . With an opening angle cut of ~ 180 mrad, a S/B ratio of ~ 12 is obtained while preserving $\sim 50\%$ of the signal. Note that this dramatic improvement is achieved by the electron-id capability of the inner detector. The π rejection factor does not play a crucial role here. As deduced from the numbers quoted in Table 3, a moderate π rejection factor of ~ 100 will add ~ 3 fake electrons to the 9 genuine electron hits in the inner detector. The consequence will only be a somewhat stronger reduction of the signal by random close hit cut. In other words, we can tolerate a low π rejection factor as long as it adds a small number of “electron” hits compared to the number of genuine electron hits in the inner detector. The requirements of the inner detector are therefore very different from those of the tracking system: the inner detector requires very high electron efficiency and can tolerate a moderate π rejection whereas for the tracking system the requirements are just the opposite, as discussed in Section 2.

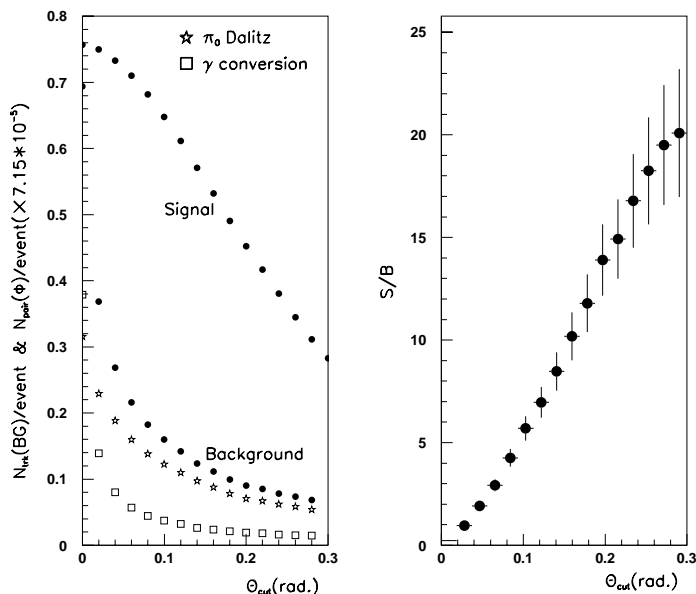


Figure 8. Left panel: absolute yield of the signal pair and background tracks per event surviving the close hit cut as a function of the opening angle cut value, assuming perfect e-id in the inner detector. Right panel: same for the S/B ratio.

3.5. Benefits of Veto Area.

Fig. 8 shows that for large opening angle cuts $\theta > 200$ mrad, the remaining background is mainly due to tracks from π^0 Dalitz decays. The conversions are almost eliminated to the level of a few percent. However, both components seem to survive even larger cuts. This is due to the fact that the partner we are seeking is outside the fiducial acceptance of the central arms. This is demonstrated in Fig. 9 which shows the location of the

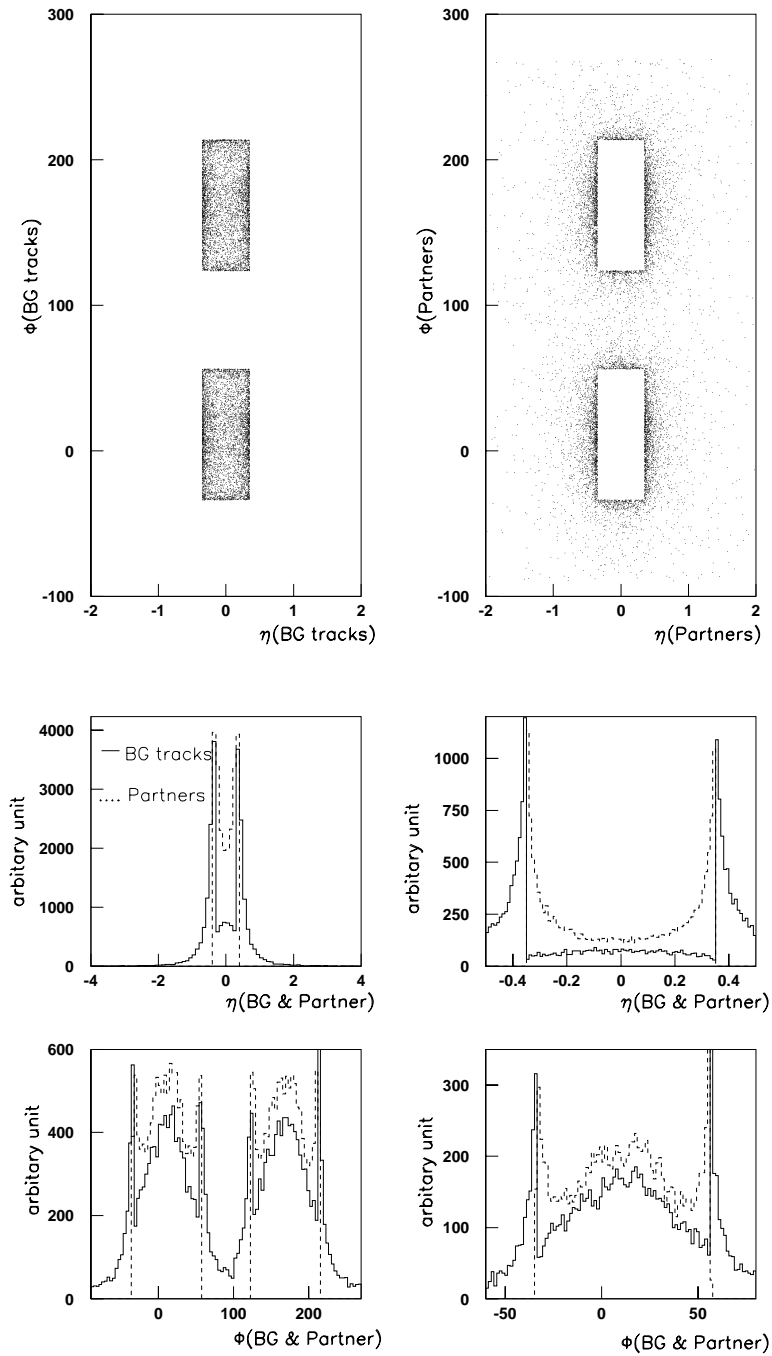


Figure 9. Location of the background tracks (upper left panel) and their partners (upper right panel) when the partner is outside the fiducial acceptance, $|\delta\eta| \leq 0.35$ and $\delta\phi \leq 90^\circ$. The lower panels show their distributions in η and ϕ .

background tracks (upper left panel) and their partners (upper right panel) when the partner is outside the fiducial acceptance, $|\delta\eta| \leq 0.35$ and $\delta\phi \leq 90^\circ$. The lower panels show their distributions in η and ϕ . One can clearly see that the background tracks and their partners mostly sit close to the boundaries of the fiducial acceptance. Therefore, the background rejection could be improved by adding a **veto area** to the inner detector

i.e. by increasing its acceptance beyond that of the central arms. In this subsection we study the additional benefit in the S/B ratio which we may expect from such a veto area. We gradually increase the acceptance both in the azimuthal direction, from $\delta\phi \leq 90^\circ$ to $\delta\phi \leq 120^\circ$ in steps of 10° , and in pseudo-rapidity, from $|\delta\eta| \leq 0.35$ to $|\delta\eta| \leq 0.50$ in steps of 0.05. The results are shown in Fig. 10. The figure shows (as in Fig. 8) the absolute yield of the signal and background and the S/B ratio for various acceptances of the inner detector. As before, for this calculation the inner detector has perfect spatial resolution and perfect e-id.

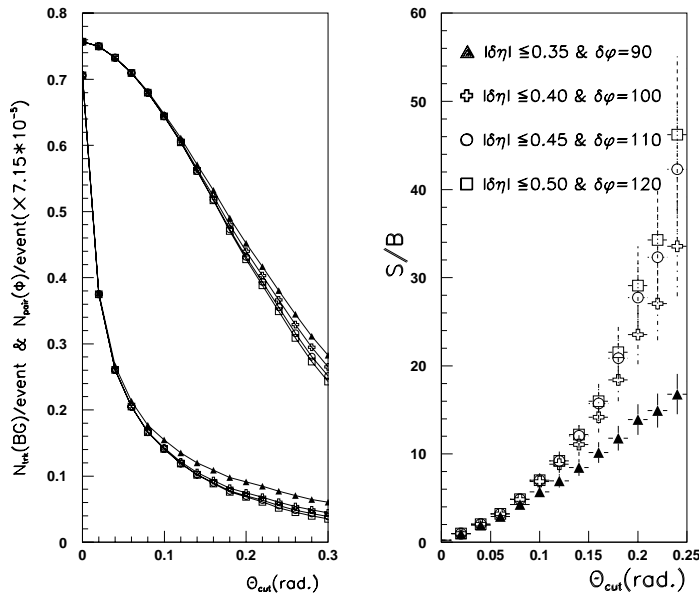


Figure 10. Left panel: absolute yield of the signal pair and background tracks per event surviving the close hit cut as a function of the opening angle cut value, assuming perfect e-ID in the inner detector. Right panel: same for the S/B ratio. The different symbols refer to different acceptances of the inner detector as shown in the right panel.

From the figure one can see that most of the improvement in the S/B ratio occurs already with a modest increase of the acceptance to $|\delta\eta| \leq 0.40$ and $\delta\phi \leq 100^\circ$. With an opening angle cut of ~ 180 mrad, it allows us to reach a S/B ratio of ~ 20 and a further increase of the veto area brings only a relatively small improvement.

3.6. Double Hit Resolution

From the results of the last section it seems that we have reached the goal. However, the study so far relies on an ideal detector. The most critical assumption is the perfect spatial resolution of the inner detector or more precisely the implied perfect double hit recognition (dhr). The importance of the dhr is clearly illustrated in Figs. 6-8 where one sees that a sizable fraction of the rejection occurs at very small opening angles.

In this section we show how much the S/B ratio is affected by assuming various levels

of dhr in the inner detector. The procedure here is as follows:

- If the distance between two hits in the inner detector is larger than the dhr, they are assumed to be recognized as two hits. Otherwise they are merged into one hit. However, they can still be recognized as a double hit by exploiting the analog response of the detector. In the present study we have assumed a 50% probability of recognition of merged double hits.
- The rest of the procedure remains unchanged, namely we consider an inner detector with veto area, ($|\delta\eta| \leq 0.40$ and $\delta\phi \leq 100^\circ$), π -rejection = ∞ and electron efficiency = 100%, we remove tracks forming a pair with $m < 130$ MeV in the outer detectors, we remove tracks with no matched hits in the inner detector and we then apply the close hit cut considering only electron hits in the inner detector.

We have considered the following cases: dhr = 0.0 mrad (i.e. the perfect case discussed so far), 10.0 mrad, 20.0 mrad and 30.0 mrad.

The results of the calculations are shown in Fig. 11. The price in S/B is tremendous. With a dhr of the order of 20-30mrad, the S/B ratio is down to 1-1.5, more than one order of magnitude compared to the values reached in the previous section. This is not a surprising result. As stated above, we need to reject conversions and π^0 Dalitz decays at least at the 90% level and consequently the probability to recognize merged hits must also be at least at the 90% level.

3.7. Summary of Monte Carlo Studies

Table 4 summarizes the S/B ratios presented in the previous sections. .

Table 4
Summary of S/B Results

		S/B
Present configuration		1/7
B = 0 at r \leq 60cm		1/5
B =0 + Inner detector:	no e-ID (cut with all hits)	1
	no e-ID (cut with single hits)	2
	e-ID	12
	e-ID + veto area	20

In order to fulfill its main goal of rejecting the background electron tracks, the inner detector must have an excellent electron identification capability (efficiency larger than 90%). This necessarily implies an excellent dhr (at least 90% probability to recognize merged hits). On the other hand only a moderate π rejection factor is required (a rejection

factor of 100-200 is sufficient). Finally an acceptance slightly larger than that of the central arms is highly desirable (for example with a coverage of $|\delta\eta| \leq 0.40$ and $\delta\phi \leq 100^\circ$).

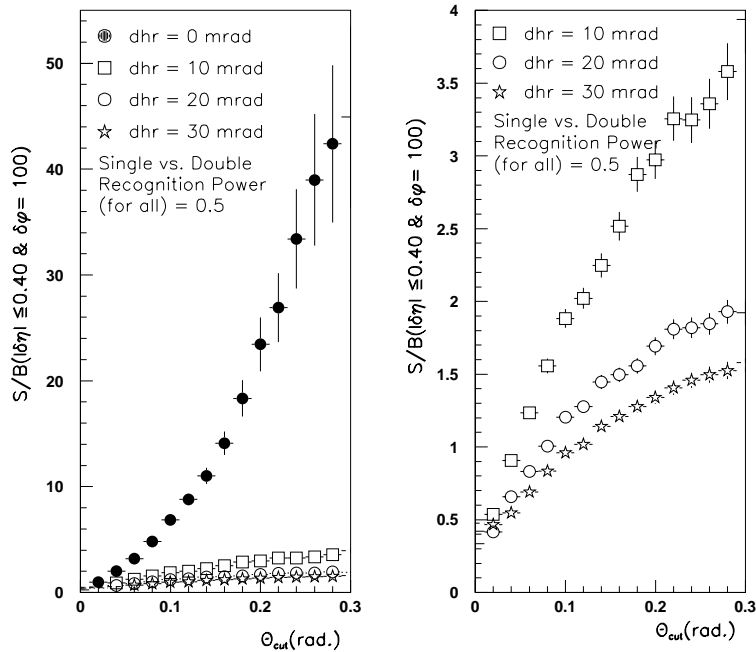
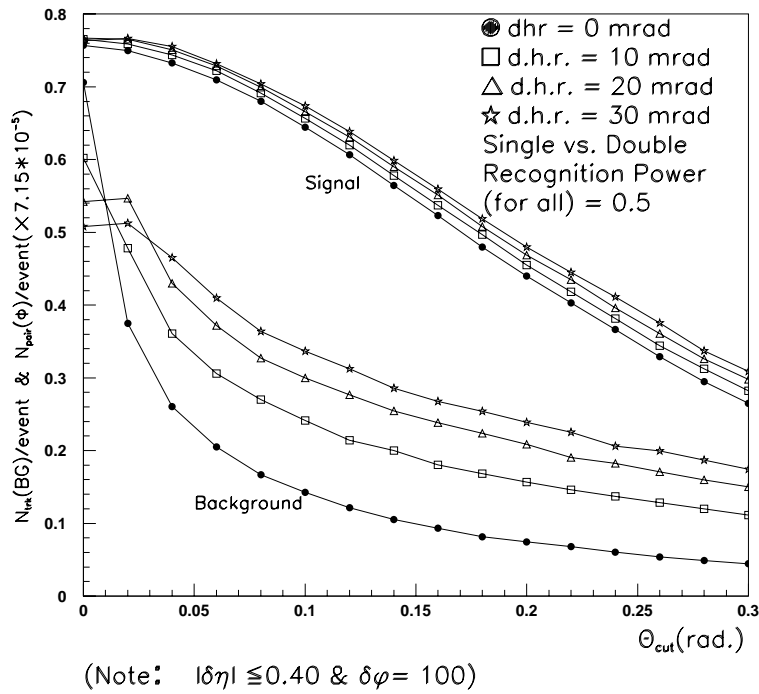


Figure 11. Signal, Background and S/B ratio for different dhr.

PART TWO: UPGRADE SCHEME

4. GENERAL CONSIDERATIONS

Based on Part One and general considerations the HBD has to satisfy the following requirements:

- Electron identification with an efficiency $> 90\%$.
- Very good double hit resolution or more precisely a double hit recognition better than 90% when hits are closer than the dhr.
- π rejection factor as low as 100-200.
- It has to fit within the radial distance $10 \geq r \leq 60\text{cm}$ and cover a slightly larger acceptance than the PHENIX central arms.
- It must have a very low radiation budget, of the order of 1% of a radiation length.

The HBD must be located close to the IR, after the MVD, in the region where the main magnetic field can be compensated by the additional magnet coil. We assume that all particles have almost straight trajectories in the region of compensation. We also assume that the space occupied by this detector is $\sim 50\text{cm}$, in the region from $R=10\text{cm}$ to $R=60\text{cm}$ covering the acceptance $|\eta| < .40$ and 100° in ϕ in each PHENIX central arm.

Good π rejection over a broad range of p_T can be achieved by a Cherenkov detector with a gaseous radiator. Such a detector will also fulfill the requirement of radiation thickness. A mirror-type RICH detector in the center of PHENIX is very difficult or nearly impossible to implement. We thus consider here a scheme similar to the one suggested in [1] and tested in [2,3] in which Cherenkov light from particles passing through the radiator is directly collected on a photosensitive cathode plane forming a circular blob image, not a ring as in a RICH. In this configuration all charged particles pass through the detection volume.

It is clear that in the high particle density environment of a central Au-Au collision the best option is to build a Cherenkov detector blind to all particles except for electrons, i.e. a Hadron Blind Detector (HBD). Since particles traverse the detector volume, TMAE cannot be used as a photosensor, because it requires a significant absorption region where charged particles produce considerable ionization. A good alternative to TMAE is the thin *CsI* photocathode which is widely used [4] since a few years.

As for any Cherenkov detector, a large number of photoelectrons is crucial for high efficiency. Because of the limited space available, the only efficient way to increase the number of photoelectrons per particle is to increase the bandwidth of detectable Cherenkov photons. A large number of photons is also crucial for a good double hit recognition (dhr).

5. MAIN ELEMENTS

In this section we discuss properties of the different elements which can be used in the HBD.

5.1. *CsI* photocathode configuration

A typical *CsI* photocathode consists of a layer of *CsI*, typically one micron thick, evaporated onto a thin conductive substrate. The electrons produced by photons in *CsI* can be extracted in different directions with respect to the photocathode plane. That determines how the electron gets into the detector volume where it is amplified. Three different types can be found in the literature. We denote them as “Reflective”, “Transmissive” and “Semitransparent” and they are sketched in Fig. 12. Those notations are not necessarily conventional. The quantum efficiency (Q.E.) strongly depends on the

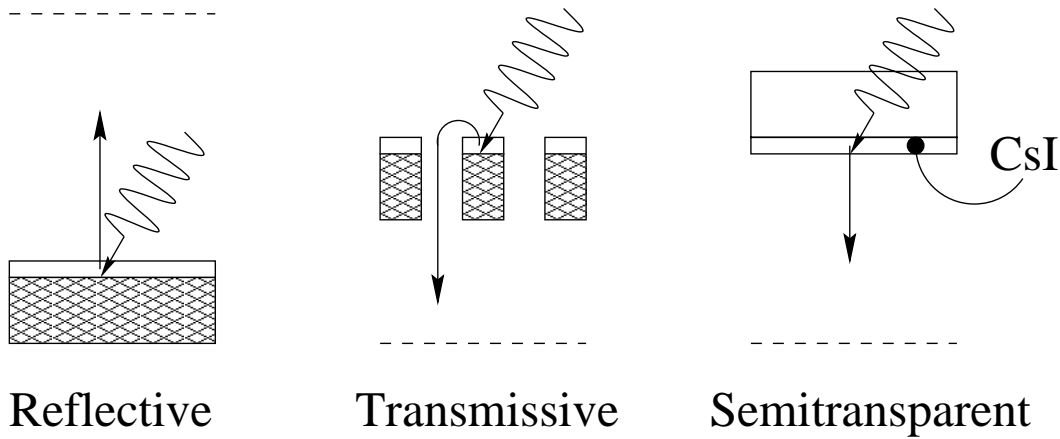


Figure 12. Three different types of *CsI* photocathodes.

configuration. The results, reviewed in [5], are plotted in Fig. 13 vs. photon energy. Advantages and disadvantages of each type are discussed below.

5.1.1. Reflective

The electron is extracted into the same volume where the incident photon comes from. The amplifier has to be on the same side of the Cherenkov radiator.

Advantages

- The full area of the detector is sensitive to photons.

Disadvantages

- *CsI* is exposed to avalanche photons.
- Only one single stage of amplification is possible.
- The detector gas must be transparent.

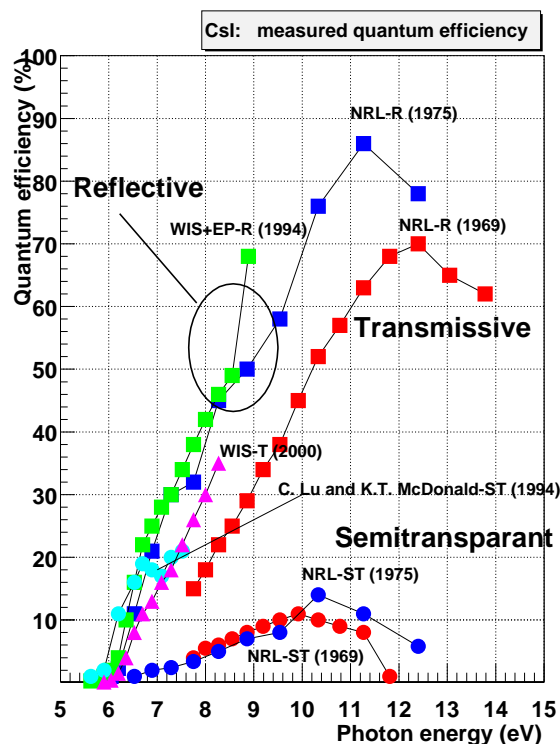


Figure 13. CsI quantum efficiency vs. photon energy.

5.1.2. Transmissive

The electron is extracted into the same volume where the incident photon comes from, but it gets turned around by an electric field and pulled through holes in the photocathode.

Advantages

- *CsI* is totally screened from photons produced in the avalanche.
- Multiple amplification stages are possible.

Disadvantages

- Photocathode working area is reduced by ($\sim 25\%$) due to holes.
- Detector gas must be transparent.
- Extraction field and amplification fields are not decoupled.

5.1.3. Semitransparent

The photon reaches the *CsI* through a window and electrons are extracted from the opposite side of the photocathode. Since *CsI* is an insulator, a thin metal layer ($\sim 30\text{\AA}$ of *Cr*) has to be evaporated between the window and the *CsI*.

Advantages

- Detector gas is totally decoupled from the radiator gas.
- Multiple amplification stages are possible.

Disadvantages

- Low quantum efficiency of the photocathode.
- UV-transparent window required.
- Additional background from Cherenkov light from the window.

From the discussion in this section it is clear that the “Transmissive” configuration is

preferable over the other two since it has a relatively high quantum efficiency and allows to screen the CsI from the avalanche. Other options have also to be considered, but their disadvantages could be more difficult to overcome.

5.2. Radiator gas choice

The following gas properties have to be considered:

- Transparency in vacuum and extreme ultraviolet (VUV-EUV) band where the CsI photocathode is sensitive.
- Gas refraction index in the region of transparency and its chromatic aberration.
- Scintillation properties of the gas.
- Radiation thickness.

5.2.1. Optical properties of gases

Only a limited number of gases have a low enough γ_{th} value to radiate a significant number of photons and stay transparent in the VUV – EUV range. Possible radiator gas candidates are listed in Table 5. One would clearly give preference to the gases with

Table 5

Radiator gases. N_0 is estimated assuming linear extrapolation of the CsI Q.E. into the region above 12eV. $\Delta\theta_{sat}$ is the chromatic aberration from ~ 6 eV to $E_{cut-off}$. The π rejection factor is calculated from the number of pions with momentum above γ_{th} . The momentum distribution is taken from HIJING

Gas	$\langle n \rangle$	γ_{th}	θ_{sat} <i>mrاد</i>	$\Delta\theta_{sat}$ <i>mrاد</i>	$E_{cut-off}$ <i>eV</i>	$N_0 = \int(Q.E.)dE$ <i>cm⁻¹</i>	π rejection
CH_4	1.000444	34	30	1.6	8.5	185	3000
CF_4	1.000620	28	36	1.8	11.5	936	1300
N_2	1.000296	41	24	1.2	9	255	10000
He	1.000035	120	8	1.5	11(?)	796	> 10000
Ne	1.000067	86	12	1.3	15	2664	> 10000
Ar	1.000283	42	24	3.3	9	255	10000

higher cut-off energy ($E_{cut-off}$) because the CsI Q.E. grows with photon energy as shown in Fig. 13, and therefore the number of detectable photons increases. Note that in gases with larger refractive index n (or low γ_{th}) the photon yield, which is given by $N_0/\gamma_{th}^2 \times L$, is larger. But at the same time the size of the blob is also larger because it is determined by the Cherenkov angle θ_{sat} . That unavoidably increases the pile-up probability of blobs from close electrons, making the dhr more difficult.

5.2.2. Scintillation properties of gases

Several gases mentioned in Table 5 scintillate. The scintillation properties of the noble gases in liquid (e.g.: [6]) and gaseous phase were studied for calorimetry and optical readout of gaseous detectors, respectively. The studies were usually done for high Z gases like *Ar*, *Kr* and *Xe*, used in calorimetry. We did not find data for *Ne*, but from the systematics one can say that all noble gases scintillate in the liquid phase. The photon yield is comparable to NaI ($\sim 10^4$ photons/MeV), the scintillation peak wavelength grows with Z of the gas (130nm for *LAr* and 175nm for *LXe*) and the decay time is short, from few to dozens of nanoseconds. It is also known that impurities in the gases dramatically reduce the light yield by offering additional channels of deexcitation.

The scintillation of carbohydrates was studied in [7] and found to be negligible.

Tetrafluoromethane (*Freon* – 14, CF_4) is also a scintillator. Its scintillation properties were studied by several groups [7,8], with consistent results. The scintillation spectrum is shown in Fig 14. There is a line at 163nm and a continuum above 220nm. Because of the

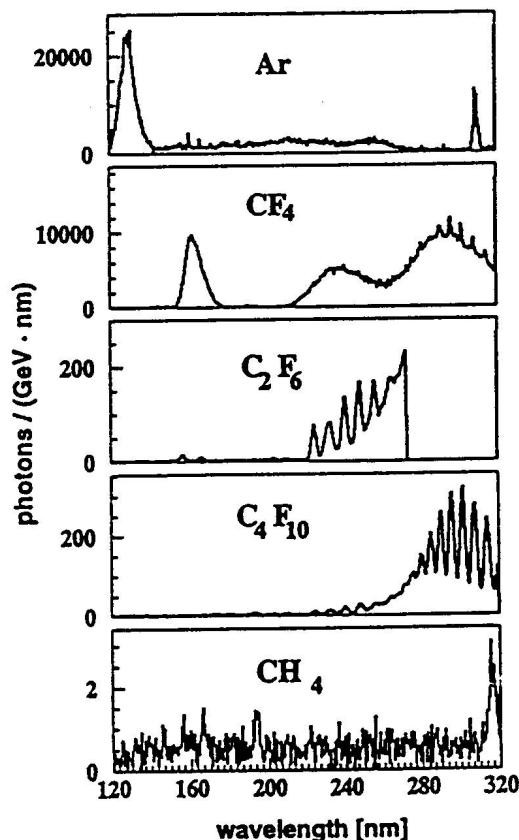


Fig. 2. Photon yield for various scintillating gases excited by ^{16}O ions of $E_{\text{kin}} = 80$ MeV. Intensities are normalized with respect to constant energy loss. A systematic error of about 50% has to be attributed to the absolute yield.

Figure 14. Scintillation spectra of fluorocarbon from [7].

latter, the HADES experiment abandoned the CF_4 option for their detector [7]. However, with a CsI photocathode this continuum falls below the CsI sensitive region (see Fig. 13) and therefore is irrelevant. The CsI is sensitive to the line at 163nm with a Q.E. around 20%-30%. The integrated yield of photons under the peak is 100-200 photons per MeV of deposited energy. The average energy loss of a MIP in CF_4 is 7 keV/cm at NTP.

Since scintillation occurs uniformly in 4π whereas Cherenkov light is emitted in a very narrow cone ($36mrad$ for CF_4 , see Table 5) a considerable reduction of the scintillation background can be achieved by installing shades. We performed a simple simulation to determine the number of photoelectrons produced by the scintillation in CF_4 with a schematic detector design as shown in Fig. 15. Radial shades 5 cm high and with 5cm

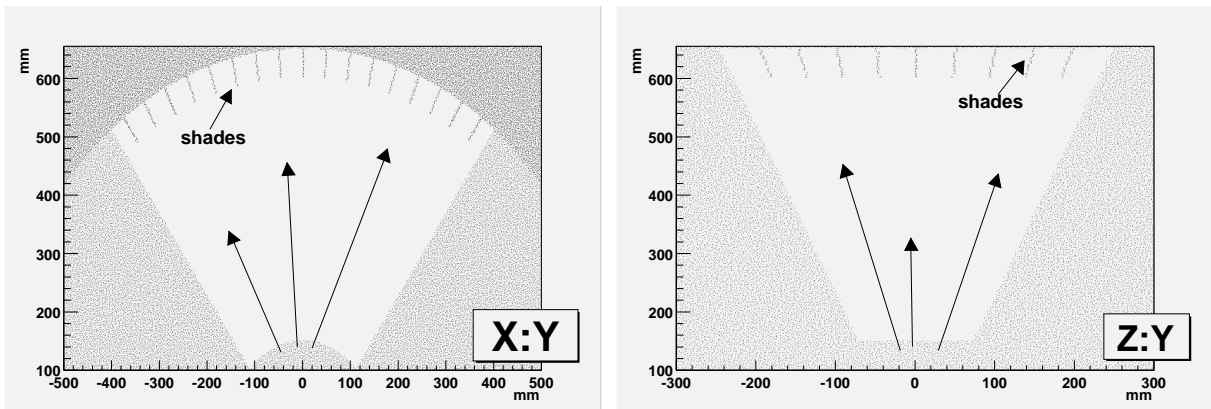


Figure 15. Cut view of the detector in two projections with shades.

spacing from each other in both directions were added close to the photosensitive cathode in order to stop photons coming from scintillation. Simulations were performed with and without shades assuming a scintillation yield of 200 photons/MeV. The results are shown in Fig. 16. Without shades one gets an average number of 0.007 photons per square

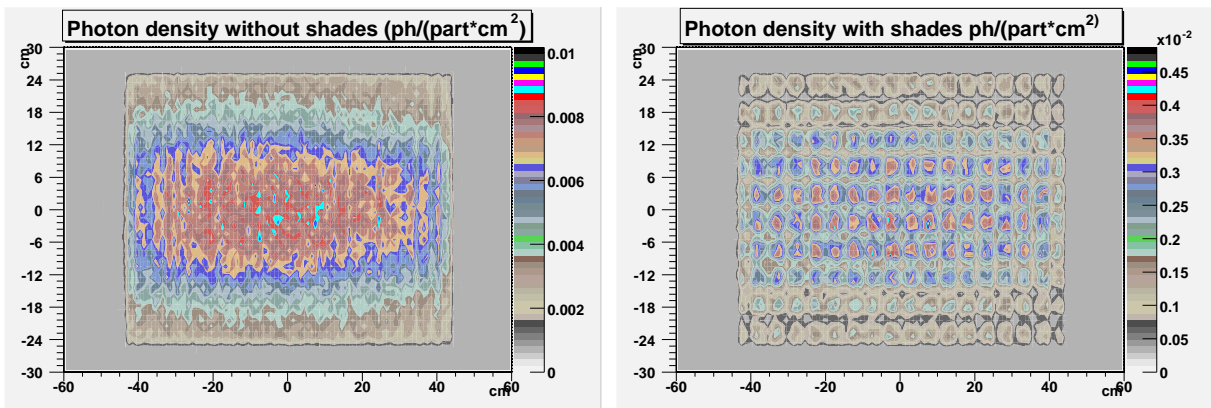


Figure 16. Photon density per cm^2 on the photocathode and per MIP from the scintillation of CF_4 , without shades (left panel) and with shades (right panel).

centimeter per particle. Adding shades reduces the background by a factor of 3 without any optimization of the shade configuration. With 250 charged particles and a *CsI* Q.E. of 30% we obtain ~ 0.15 photoelectron per cm^2 . Note that in this exercise, the values used for scintillation yield, number of particles in the volume of the detector and quantum efficiency of *CsI* represent the worst scenario. The blob size in this detector configuration has a radius of $50cm \times 36mrad = 1.8cm$ and the number of Cherenkov photons in the blob $(N_0 \times L)/\gamma^2$ is close to 60. The signal to background ratio in the blob is equal to $60/(0.15 \times \pi R^2) \approx 30$. Therefore one can conclude that the scintillation of CF_4 is not a killing factor prohibiting the use of this gas with *CsI* photocathode.

Another benefit may come from the timing properties of the CF_4 scintillation process. Those were not studied. Since the scintillation of molecular gases is usually slow (order of ~ 100 ns decay time) a further significant suppression of the background can be obtained, provided that the HBD is a fast device (~ 10 ns response time).

Among the options for the radiator gas discussed in this section the choices below are the most interesting ones:

CH₄ This is a conventional gas used in RICHes. Methane can be used as a detector gas (in mixtures) thus offering the possibility to use it in a windowless configuration. *CH₄* itself and its products are completely harmless for the detector and *CsI*. Mixing this gas with others is not a problem. The main drawback of *CH₄* is that its cut-off energy is low $\sim 8.5eV$ and consequently its photon yield is relatively low.

CF₄ Good choice from many points of view: high photon yield, known to be a chamber working gas [3,14,15], acceptable size of the blob ($\theta_{sat} = 36mrad$). *CF₄* is a scintillator. However, as discussed previously, this is not a killing factor. The main concern is that the Q.E. of *CsI* was reported to decrease with time in presence of *CF₄* [2], although in a similar measurement performed by [3] no effect was mentioned. We discuss later a technique which helps to avoid this particular problem.

Ne Can be a very interesting option due to its much smaller blob size ($R_{blob} = \theta_{sat}L = 6mm$) and high photon yield due to its transparency deep into the EUV region. To take advantage of the very large bandwidth, we must adopt a windowless scheme. Several questions need study: i) the *CsI* Q.E. in this region is not yet known, ii) *Ne* scintillation in a pure state and in mixtures, iii) detector performance in pure *Ne* is questionable.

Mix Mixtures of *CF₄* with *Ne* or *He* are very interesting, since they can be used as a detector gas while keeping enough yield of the photoelectrons.

The choice of the radiator gas determines the detector occupancy. It can be roughly estimated as $N_e(\pi\theta_{sat}^2)/(\Delta\eta\Delta\phi)$, where N_e is number of electrons (approximately 10 in a central collision) in the acceptance ($\Delta\eta = 0.7$, $\Delta\phi = \pi/4$) of one central arm and θ_{sat} of the gas is taken from Table 5. For CF_4 one gets an occupancy $\sim 4\%$ for a central Au-Au collision.

5.3. Amplification element

The high γ_{th} of the radiator gas ensures a large π -rejection factor and very low yield of Cherenkov photons from hadrons. This is a desired property since we want to minimize the HBD response to hadrons.

On the other hand, the HBD should be sensitive to signals produced by a low number of photoelectrons. The total number of photoelectrons per one readout channel depends on the radiator gas and the channel size. This will be discussed later in detail. However, since the initial number of photoelectrons is small, and can be shared between several channels we require that the HBD detection element should reach a multiplication factor of $\sim 10^4$, or a few times 10^4 .

The detector has to sustain a broad dynamic range of signals up to those produced by highly ionizing particles, with a negligible discharge rate. The discharge-free operation of the detector is essential because the CF_4^+ radicals produced in the breakdowns can accelerate the aging of the detector.

We briefly discuss here several detector options:

PPAC In *Parallel Plane Avalanche Chambers* the effective multiplication for a charged particle is practically one order of magnitude lower than for a single electron since only ionization electrons produced in the vicinity of the cathode do get the full amplification. However the PPAC has a proportional response and in the presence of heavily ionizing particles they are known to go into a sparking regime [2,10,11] since the breakdown quenching mechanism in PPAC is basically absent.

MWPC *Multiwire Proportional Chambers* do not have that problem since their response saturates with increasing charge and the breakdown point is not reached. However we will lose the “blindness” to hadrons since a single stage MWPC alone will be practically 100% sensitive to charged particles.

MPD *Micropattern Detectors* (or combination of those with a MWPC) is a promising choice. In a micropattern detector the distance between electrodes is short (typically less than $100\mu m$) and a MIP leaves there a very small primary charge. Among the existing types of micropattern detectors (MSGC, MICROMEGAS, MICROCAT/WELL, MICRODOT, GEM see [9] and references therein) none of them

reaches the desired gain before breakdown in a single stage. Typically all of them turn into a spark regime at a gain of 10^3 in the presence of heavily ionizing particles.

One of the micropattern detectors, the GEM (Gas Electron Multiplier) mentioned above, can be used in a multistage configuration. The structure of GEM is such that the signal is transferred to the opposite side of the GEM and with an appropriate electric field can be fed into another detector. Results using 2-3 (standard) and up to 5 GEMs can be found in the literature. Among the micropattern detectors multistage GEM allow to achieve the highest gains before breakdown is reached, compared to others MPDs.

A gas multiplication factor of 10^4 was achieved with a double GEM configuration in the presence of highly ionizing particles (admixture of ^{220}Rn isotopes emitting α with $E=5.6\text{MeV}$) before any significant breakdown rate was reported in Ar/CO_2 gas mixtures which are not optimal for best multiplication and stability [9,12]. There is also a variety of data on triple GEM operation in different gas mixtures including CF_4 showing higher gain. That allows us to hope that with a multi-GEM detector or multi-GEM + Wire Chamber the desired gain of $\sim 10^4$ can be achieved at a negligible breakdown rate.

GEMs are cheap, commercially available and can be produced up to a size of $\sim 30 \times 30 \text{ cm}^2$.

5.4. Detector gas choice

In the sketches shown in Fig. 12, the detector and radiator volumes are the same for the “Reflective” and “Transmissive” types of photocathodes. However it is possible to decouple these two volumes by introducing a thin window between the two volumes. The window material choices are discussed below. Installing a window has obvious drawbacks: more complicated design, additional radiation length, and more importantly, the window is an additional source of Cherenkov photons produced in the window.

In the “Semitransparent” option where the two volumes are decoupled, the detector working gas can be freely chosen, and optimized for best performance. However, the obvious disadvantages mentioned in 5.1.3 make this option practically impossible to implement, and therefore it is not discussed further.

With a window option the working gas can be different from the radiator gas, but it still has to be EUV transparent. One should note that the photoabsorption edge in the gas mixtures (cut-off energy) is practically dictated by the less transparent component of the mixture. In addition one would like to use gases with low dE/dx to minimize the response to charged particles traversing the detector volume.

Some detector gases are listed in Table 5. We add a few more options and focus on their properties as detector gases. These are summarized in Table 6.

For the detector gas selection one has to take into account the fact that the extraction

Table 6

Detector gases. n_p is the number of primary clusters per cm, n_T is the number of primary electrons in those clusters.

Gas	$E_{cut-off}$ eV	dE/dx (keV/cm)	n_p cm^{-1}	n_T cm^{-1}	Detector	
					working gas	quencher
CH_4	8.5	1.48	25	53	–	very good
C_2H_6		1.15	41	111	bad	excellent
CF_4	11.5	7	51	100	–	very good
N_2	9	2.28	22	63	satisfactory	satisfactory
He	11(?)	0.32	4.2	8	good	very bad
Ne	15	1.56	12	43	excellent	very bad
Ar	9	2.44	23	94	excellent	very bad
CO_2		3.01	36	91	–	good

of electrons from the photocathode into vacuum (the CsI Q.E. shown in Fig. 13 was measured for this case) and into a gas atmosphere are different. In some gases the electrons coming out of the cathode can be reflected back and lost. It has been shown [11] that for CH_4 the losses are small but for some mixtures of noble gases they can reach dozens of percent, which is a significant factor for the gas choice. In general, the electron extraction into a molecular gas atmosphere is more effective than into atomic (noble) gases. It has also been shown that the extraction in the case of a “Transmissive” photocathode is more effective when the field above the cathode is close to zero.

It was already stated in 5.1 that CF_4 or $CF_4 + Ne$ gases are the best choices for Cherenkov radiators. From Table 6 one can see that they can be used as detector gases too. It was also mentioned that CF_4^+ can reduce the CsI Q.E.. This effect can be significantly or even totally suppressed using a gating technique, but applied not to the incoming electrons (as it is usually done in TPCs) but to the ions traveling back to the photocathode at a much slower speed. For example, in a multi-GEM detector gating can be achieved by changing the transfer field between the first and the second GEM or by changing the GEM voltage or the field between the first GEM and entrance grid. Pulses of the order of $\sim 100V$ and $\sim 10\mu s$ are needed and can easily be obtained from many commercial power supplies. More studies are needed because up to now no study of GEM gating exists, and in general, gating might cause a problem to highly sensitive electronics.

5.5. Window choice

A window might be needed if a “Semitransparent” photocathode is used or if the radiator and detector volumes have to be decoupled. Among the window materials commercially available [16] the fluoride windows are the most interesting. Their properties are summarized in Table 7. Fused quartz window is also shown for comparison.

Table 7
Window materials and properties

Material	$E_{cut-off}$ <i>eV</i>	n	X_0 <i>cm</i>	Comment
<i>LiF</i>	11.9	1.38-1.90	14.9	slightly hygroscopic, fragile
<i>MgF₂</i>	11.3	1.43-1.90	10.	very little hygroscopic
<i>CaF₂</i>	9.9		7.	fragile
<i>SiO₂</i>	7.5(?)	~ 1.5	11.7	a glass

From the table above one can conclude that *LiF* is the best choice for the window. It can be produced to a size of $\sim 100cm^2$ at thickness of $0.5mm$ [2] and also has the largest X_o value. It is known that *LiF* window can be exposed to air for quite a long time without deteriorating its EUV optical transparency. Too long exposure may cause some changes. *LiF* is fragile, difficult to handle and relatively expensive.

Another choice is *MgF₂* which has almost the same transparency, is easier to handle, less fragile and insensitive to atmosphere. *MgF₂* has lower X_o and slightly larger refraction index which results in more photon yield from charged particles passing through it.

As mentioned previously the main disadvantage of a window is the Cherenkov light it produces. *LiF* has the lowest refraction index, its photon yield is smaller and a certain fraction of it will be internally reflected as studied in [2]. The simulations in [2] were done for a limited bandwidth dictated by the choice of *CH₄* as a detector gas, yielding ~ 0.6 photons per charged particle for any angle of incidence, in agreement to the measured value. Extrapolation of this result to the *CF₄* bandwidth gives $\sim N_0/\gamma_{th}^2 = 0.6 \times (936/185) \cdot (34/28)^2 \approx 5$ photons per charged particle. The estimate is conservative. The photon yield suppression from the window due to total inner reflection is more effective when the refraction index is larger. The latter grows with photon energy (reaching almost $n = 2$ at $E_{cut-off}$ both for *LiF* and *MgF₂*). Adding shades on the inner side of the window also helps to reduce the Cherenkov light by a factor of 2-3, as discussed in [2].

If one can find two materials with cut-off energy close to *CF₄* and different refraction indices, one could in principle, construct a selective dielectric filter by evaporating multiple layers of the two materials of a given thickness (thickness is given by $(\lambda n)/(4\cos(\theta))$, where λ is the wavelength of interest, θ angle of incidence and $n(\lambda)$ refraction index). That can help to eliminate the 163nm scintillation peak of *CF₄* or to reflect back the Cherenkov light from the window which propagates in a different direction compared to the Cherenkov light from the gas radiator. This is a standard optical technique, but more study is needed for a particular implementation.

6. DETECTOR CONFIGURATION

Based on the discussions in the previous section we choose the following options for the various detector elements: i) the radiator gas is CF_4 or a mixture of CF_4 with a noble gas, ii) windowless configuration, i.e. same gas in the detector element; iil) “Transmissive” photocathode scheme; iv) triple GEM (or double GEM plus MWPC) coupled to a cathode readout. The layout of an HBD based on these elements is shown in Fig. 17. The CsI

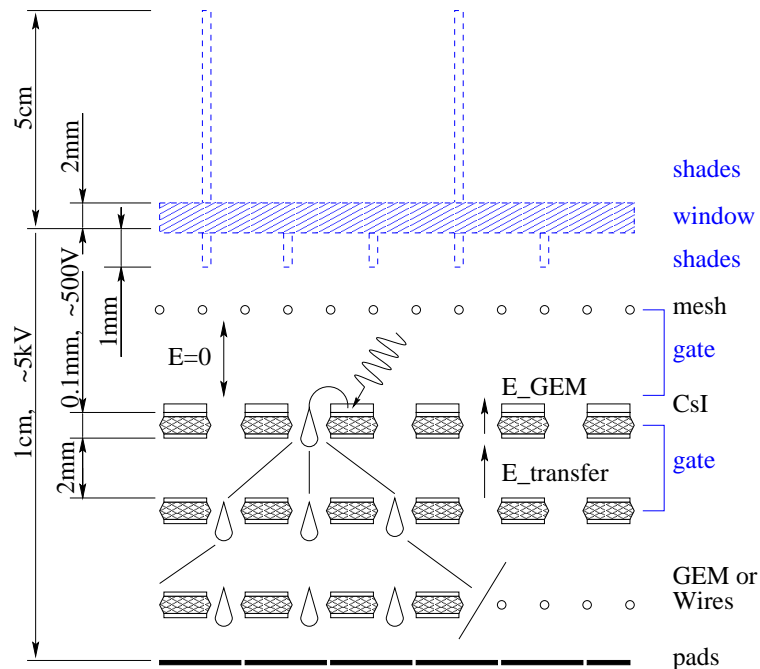


Figure 17. Possible detector configuration. Additional options are shown in blue.

photocathode is evaporated onto the first GEM with a thin gold substrate to prevent chemical reaction of the CsI with the Cu clad of the GEM. The GEM optical transparency is about 25%. A mesh before the first GEM (with an optical transparency of about 90%) is needed to ensure a zero field above the photocathode, which is the best for electron extraction in the “Transmissive” photocathode scheme [11].

The operation of a detector using pure CF_4 , CsI photocathode and three stages of GEM amplification has recently been demonstrated [13]. Fig. 18 shows the amplification curve obtained. Compared to more conventional gas mixtures, CF_4 requires higher operating voltages, but allow to reach easily gains of the order of 1000.

The relevant length for a MIP traversing the first GEM is only the distance of half a hole pitch ($< 100\mu m$) from its surface, where the electric field collects the primary ionization inside the holes. The field in the first GEM has to be high enough to effectively collect the photoelectrons from its surface and provide a high enough first stage amplification. If a

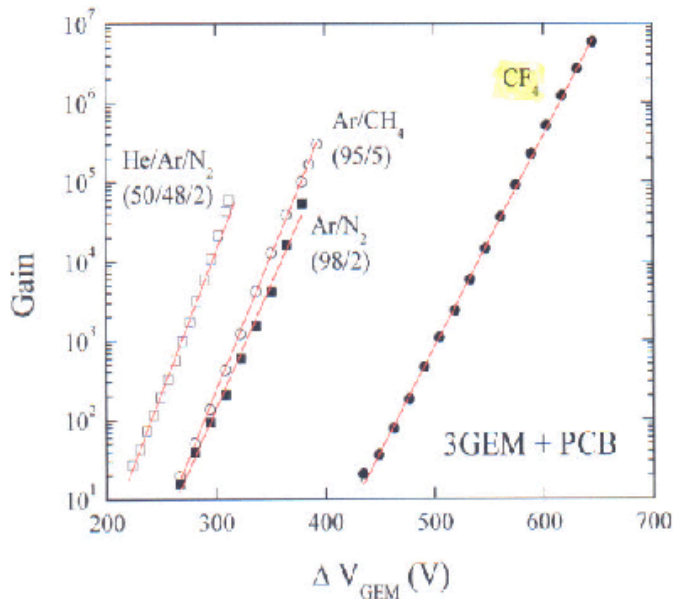


Figure 18. CF_4 amplification curve measured in a three stage GEM structure with a CsI photocathode [13].

multiplication factor of several hundreds is reached in the first GEM the energy deposition of a MIP in the gap between the first and the second GEM ($\sim 2\text{mm}$) will lead to a much smaller signal compared to that of a single photoelectron. Thus, the signals produced by the ionization of charged particles can be negligibly small.

The typical voltage at the photocathode is of the order of $3\sim 5\text{kV}$. The voltage on each GEM is about 500V . The voltage between GEMs has to be set such that it ensures an effective transfer of charges from one layer to another. Increasing the distance between the GEMs may help to spread the avalanche over a large number of holes, but results in a slower detector operation and larger energy deposition by a MIP. This spread, however cannot be very broad and depends on the diffusion in the detector gas. The last GEM can be substituted by a wire chamber if sparking free operation cannot be achieved at the desired gain. The readout is done from a pad array below the last amplification element.

Other choices are possible or additional options might be necessary, for example window/filter, shades and gating. These additional options are shown in blue in Fig. 17.

Table 8 summarizes the detector response to electrons and hadrons. We have calculated the properties and characteristics of the most attractive choices, assuming a 50cm long gas radiator. The first part of the table (Detector Configuration) lists the detector elements: gases, photocathode type, window and shades. The latter can be installed inside the radiator volume (with dimensions as discussed in 5.2.2) and/or inside the detector volume in case that a window is installed (with dimensions as discussed in [2]).

Table 8: Detector performance for different configurations and gas choices. *Photocathode* choices are Reflective, Transmissive or Semitransparent. *Shades in Rad./Det.* are shades located in Radiator / Detector volume respectively. *DHR* is the probability to resolve two electrons with zero opening angle using amplitude analysis assuming 5% inefficiency to electrons. N_e *Glob./Loc.* is the number of background electrons within the size of a blob due to scintillation (Global) and to particles passing through the window/detector, close to the center of the blob (Local). X_0 is estimated assuming the pad plane to have a design identical to the PC1 padplane (0.475% X_0). π *Rejection* see text.

N	Detector Configuration				Response to:				hadrons		π Rejection	
	Radiator gas	Photo-cathode	Detector gas	Win dow	Shades in Rad./Det.	γ_{th}	N_{pe} per e^\pm	R_{blob} [cm]	DHR	N_e Glob./Loc.		X_0 [%]
1	CF_4	Trans	same	No	No/No	28	40	1.8cm	> 90%	4 / 1	1.25	> 10^4
2	CF_4	Trans	same	No	Yes/No	28	35	1.8cm	> 90%	1 / 1	1.30	> 10^4
3	CF_4/Ne 50/50	Trans	same	No	No/No	~ 40	30	1.3cm	$\sim 90\%$	2 / 1	1.05	$\sim 10^4$
4	CF_4/Ne 10/90	Trans	same	No	No/No	~ 70	20	1.0cm	$\sim 70\%$	1 / 1	0.85	350
5	CF_4	Trans	CF_4/Ne	Yes	No/No	28	40	1.8cm	> 90%	4 / 5	1.60	700
6	CF_4	Trans	CF_4/Ne	Yes	Yes/Yes	28	35	1.8cm	> 90%	1 / 3	1.65	> 10^4
7	CF_4	Trans	CF_4/He	Yes	Yes/Yes	28	35	1.8cm	> 90%	1 / 3	1.65	> 10^4
8	CH_4	Refl	same	No	No/No	34	8	1.5cm	$\sim 40\%$	0 / < 1	0.60	> 6
9	CH_4	Trans	same	No	No/No	34	6	1.5cm	$\sim 30\%$	0 / < 1	0.75	> 2.5
10	CF_4	SemiT	any	Yes	No/No	28	10	1.8cm	$\sim 50\%$	1 / ~ 10	1.60	failed?
11	Ne	Trans	same	No	No/No	86	20	0.8cm	$\sim 70\%$? / < 1	0.85	?

The second part of the table shows the HBD response to electrons estimated for a given configuration. It includes the γ_{th} value, number of photoelectrons N_{pe} , size of the blob $R_{blob} = \theta_{sat} \times 50$ and an estimate of the dhr. N_{pe} is calculated based on numbers given in Table. 5 and approximately 35% losses due to the photocathode optical transparency and the first mesh. We assume that the shades reduce the number of photoelectrons by $\sim 10\%$, which is probably an overestimate. The estimate of the dhr, is based on the photoelectron distributions and is the probability that an e^+e^- pair with zero degree opening angle produces a signal larger than the top 5% of a single electron signal.

The third part of the table shows the detector response to hadrons: number of electrons N_e , and the radiation length. N_e is the equivalent background signal within the size of a blob. It may be localized (Local) in one pad when it comes from the ionization or Cherenkov light in a window, or uniformly spread in many pads as in the case of CF_4 scintillation (Global). For the CF_4/Ne mixtures we took the CF_4 contribution only. The radiation length budget is estimated assuming that the pad plane mechanical design is the same as that of PC1 and taking into account the materials used in all other elements including the radiator gas.

The last column contains an estimate of the π rejection factor that can be achieved. It is the number of π producing a signal below threshold divided by number of π above threshold. The threshold corresponds to the lowest 5% of a single electron signal.

Among the options listed in Table 8 the most attractive is option number 1. It is the simplest configuration, it gives around 40 photoelectrons per electron, it has excellent dhr and very high π rejection. The main open issue is the scintillation of CF_4 . We consider this option as our prime choice and options 2-9 aim at curing possible problems which may arise.

As an example, the second option significantly reduces the background from CF_4 scintillation by introducing shades in the radiator volume.

Options 3 and 4 can be explored if amplification in pure CF_4 is low or if the detector performance is unstable. Adding Ne to CF_4 would make an almost ideal detector gas mixture while keeping the number of photoelectrons high. It can be also combined with option 2. The π rejection factor remains acceptable but the dhr power decreases if too much Ne is added.

In order to improve the dhr one has to increase the number of photoelectrons. A thin window allows to recover the same N_{pe} as in pure CF_4 by decoupling the radiator and detector volumes (option 5). This has a clear disadvantage, namely the Cherenkov light from the window itself.

Again, option 5 with shades on both sides drastically improves the pion rejection (op-

tions 6 and 7). One should note that the design in this case is more complicated due to the window and shades, however the total radiation budget doesn't grow too much.

The options not mentioned in Table 8, but discussed above and shown in Fig. 17, are different types of gating in order to protect the CsI from CF_4^+ ions in case that the photocathode suffers too much from them.

Finally one can always consider a more conventional choice using CH_4 (options 8 and 9). These options have worse π rejection capabilities but more study is needed for more realistic estimates.

Option 10 demonstrates that the Semitransparent photocathode configuration doesn't give enough photons and has many additional problems. We do not consider it as a possible solution and include it for comparison only.

Option 11 with pure Ne may be an option for the HBD using CsI . However there are too many open questions like scintillation, gas gain in pure Ne CsI Q.E. at high photon energy, and electron extraction.

7. DETECTOR GRANULARITY.

Detector granularity is an important design parameter affecting occupancy, hit pile-up, dhr and last but not least cost. As mentioned in section 5.2, the occupancy for CF_4 is close to 4% for the most central Au-Au collisions at $\sqrt{s_{NN}} = 200\text{GeV}$. The shape of the blob is shown in Fig. 19 for electrons of different p_T . As one can see the edge of the blob is slightly deteriorated because of the chromatic aberration and multiple scattering. It might be further deformed due to residual magnetic field. From the experience with mirror-type RICHes, the chromatic aberration is usually [17] the dominant factor.

There are two extreme options for the detector granularity. The first one targets at the reconstruction of the position of one single photoelectron, whereas the second one aims at the reconstruction of the blob position. Advantages and disadvantages are briefly discussed here.

7.1. Single photoelectron detection option

This solution provides the best possible single hit resolution and dhr. However, it requires the highest multiplication factor in the detector and highest readout granularity. High gain is the most serious disadvantage of this scheme, since it may be difficult to achieve and it can result in faster detector aging. The second requirement might also be difficult to implement when N_{pe} is high. With 2×40 photoelectrons in the 10cm^2 area of one blob, one would need a pad size smaller than $3 \times 3\text{mm}^2$. Such a density of pads is difficult to implement. An advantage of this scheme is that it does not require analog readout.

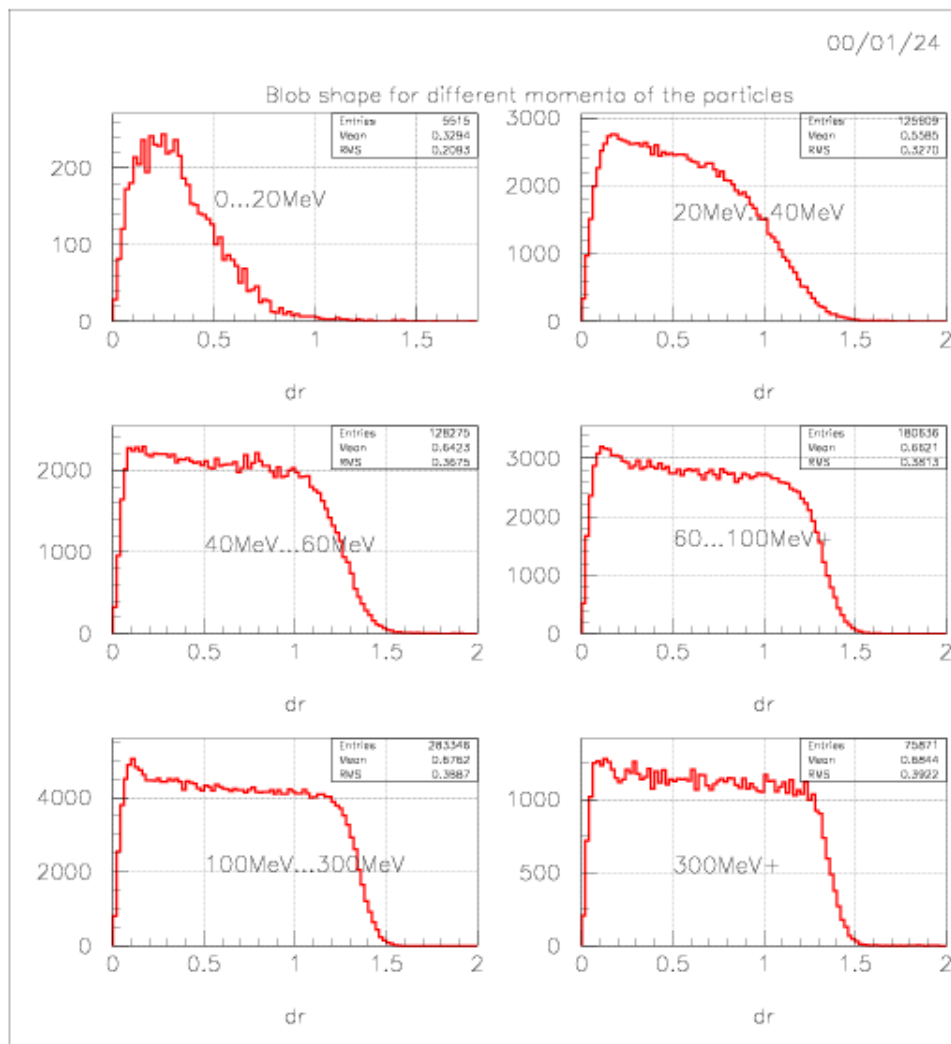


Figure 19. Shape of the blob produced by electrons of different p_T in a 40cm long CF_4 radiator. Chromatic aberration and multiple scattering are taken into account. Residual magnetic field is not considered.

This scheme might be advantageous when the N_{pe} is small (as in the case of CH_4) and a high gain in the detector is practically unavoidable. The actual shape of the blob in this case will be dictated by the low N_{pe} value.

7.2. Blob detection option

This solution, in principle, gives worse spatial resolution and dhr compared to the previous one. However, it is applicable when N_{pe} is high and the amplitude analysis helps compensate this disadvantage. This option requires lower multiplication factor in the detector, which is very important. It also results in a much smaller number of pads.

In order to get as much charge in one pad as possible, the pad size must be close to the

size of the blob. With an hexagonal pad shape this number can be smaller or equal to 3. Fine tuning can also be done by adjusting the threshold in the pads. We will show later, in 8.3, that e^+e^- pairs with an opening angle smaller than $2 \times \theta_{sat}$ are resolved with a very high probability..

There is an intermediate option when the pad size is smaller than the size of the blob. This will require a somewhat higher detector gain, but may give an additional handle for the π rejection capability if hadrons produce a significant response in the detector. One can choose the size of the pad such that an electron can never fire one single pad. At the same time the signal from hadrons is always localized (ionization or Cherenkov light in a window). This case was not studied separately.

7.3. Pad shape

As a general requirement we consider only symmetric patterns and geometries with close to 100% coverage of the detector area. Some possible pad patterns and their chevron-like modifications are shown in Fig. 20. The chevron-like modifications of the pads provide

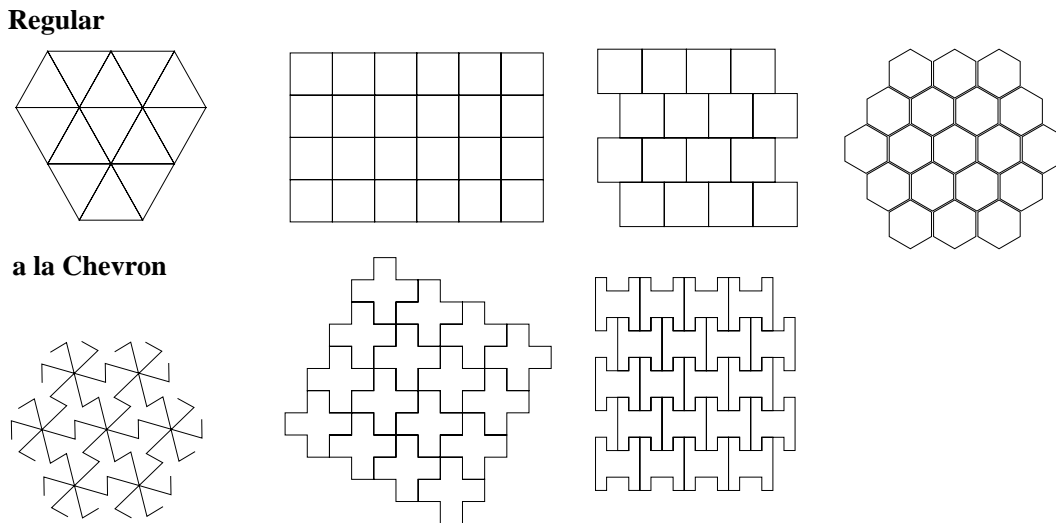


Figure 20. Possible pad shapes and their chevron modifications.

better position resolution of the hits, but are worse in dhr. Since the latter is of utmost importance for us we drop the chevron-like geometries from consideration and concentrate on compact pad shapes.

Collecting as much charge as possible in one single pad demands to avoid sharing of one hit signal between many pads. This is true for both the single photon detection and the blob detection options. From this point of view the triangular and regular square geometries are less attractive, since the number of neighbors having a common vertex is 6 and 4 respectively. Staggered squares and hexagonals pads have only 3 neighbors

with common vertex. Between these two, we prefer the latter due to its higher degree of symmetry.

8. DOUBLE HIT RECOGNITION

In this section we discuss cluster reconstruction and dhr evaluation.

8.1. Hit shape cut

The possible configurations of hit clusters are indicated in Fig. 21. The cluster notation

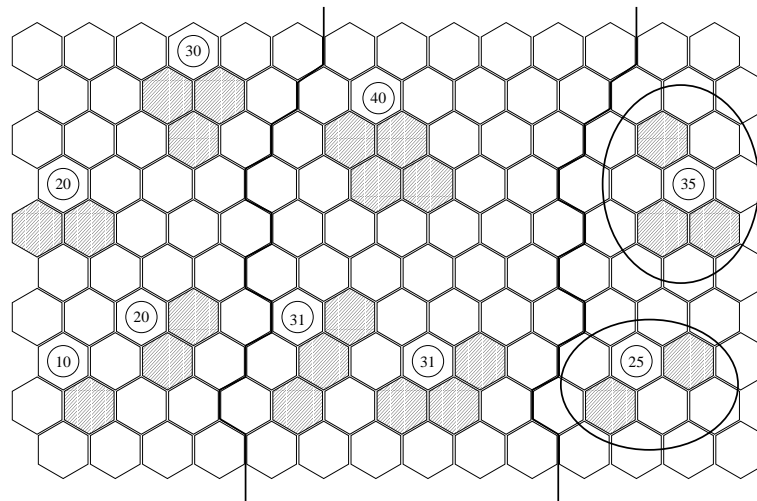


Figure 21. Cluster shape. The first digit in the notation is the number of fired pads, the second is “0” -for compact clusters “1” -for non compact clusters and “5” -for split clusters.

is a two digit number where the first digit is the number of fired pads. The second digit is “0” -for compact clusters “1” -for non compact clusters, and “5” -for split clusters. Fig. 22 shows results of a simulation of the cluster type distributions for one (top) and for a pair of electrons (bottom) in the detector volume. The opening angle of the pair was chosen uniformly up to some value where all pairs produce split clusters (type X5). Therefore only the peak heights in the top figure are meaningful. One can see that a single electron hit always produces a compact cluster (types 10,20,30). Contributions of clusters 40 and 31 are below the percent level. Thus, only compact clusters shown in the left of Fig. 21 (plus all possible rotations of them) can be taken as candidates for a single electron hits and such a cut on the cluster type provides some recognition of double hits. We will refer to this hit shape cut as the Geometrical cut.

As one can see, a cut on the hit amplitude will also help distinguishing between single and double hits. It obviously results in the loss of some single electron hits. For the dhr estimate in Table. 8, the amplitude cut was set to 5% single hit losses.

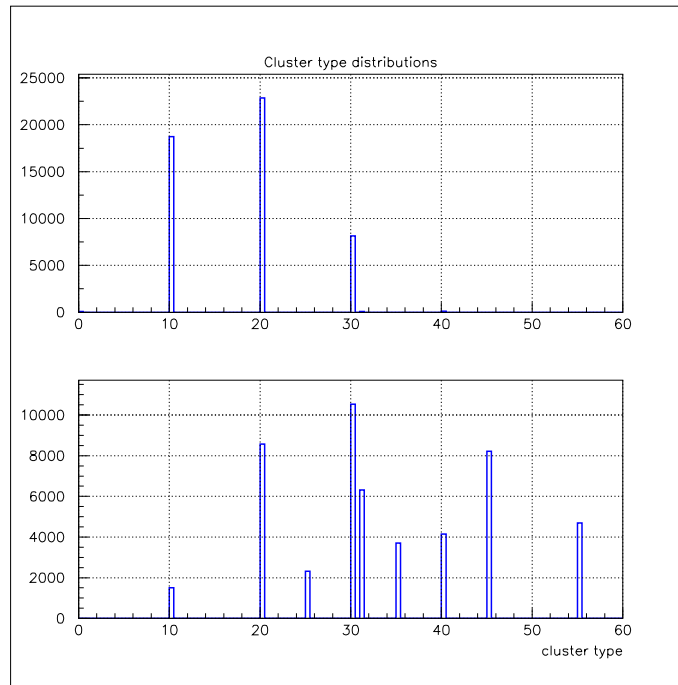


Figure 22. Probability to find a cluster of a given type produced by a single particle (top) and two particles (bottom) for $N_{pe} = 20$. The threshold setting per pad corresponds to 3 photo-electrons. Pad size is $r=1.8\text{cm}$.

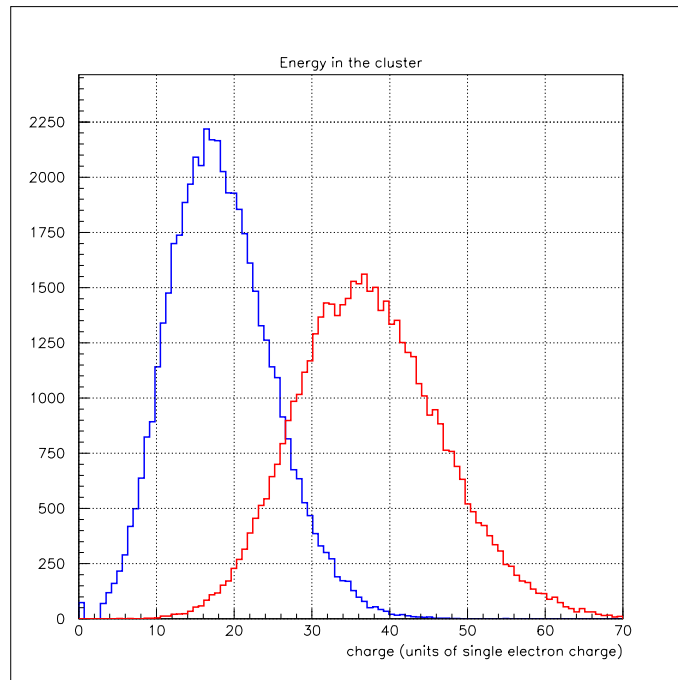


Figure 23. Hit amplitude distribution for $\overline{N}_{pe} = 20$ and 40.

8.2. Hit amplitude cut

Hit amplitude distributions were calculated assuming Poisson statistics with \overline{N}_{pe} and an exponential distribution for the single electron amplitude.

Results of the simulation for $\overline{N}_{pe} = 20$ are shown in Fig. 23. The second curve in the graph represents the same number of events with $\overline{N}_{pe} = 40$. As one can see, a cut on the hit amplitude will also help distinguishing between single and double hits. It obviously results in the loss of some single electron hits. For the dhr estimate in Table. 8, the amplitude cut was set to 5% single hit losses.

8.3. Simulation results

A sample of e^+e^- pairs was generated with uniform distance between the e^- and the e^+ in the interval $d = 0 - 7.5$ cm. The simulations were performed for $\overline{N}_{pe} = 10$ and 20. The flat curves in Fig. 24 show the initial distribution of distances between the electrons.

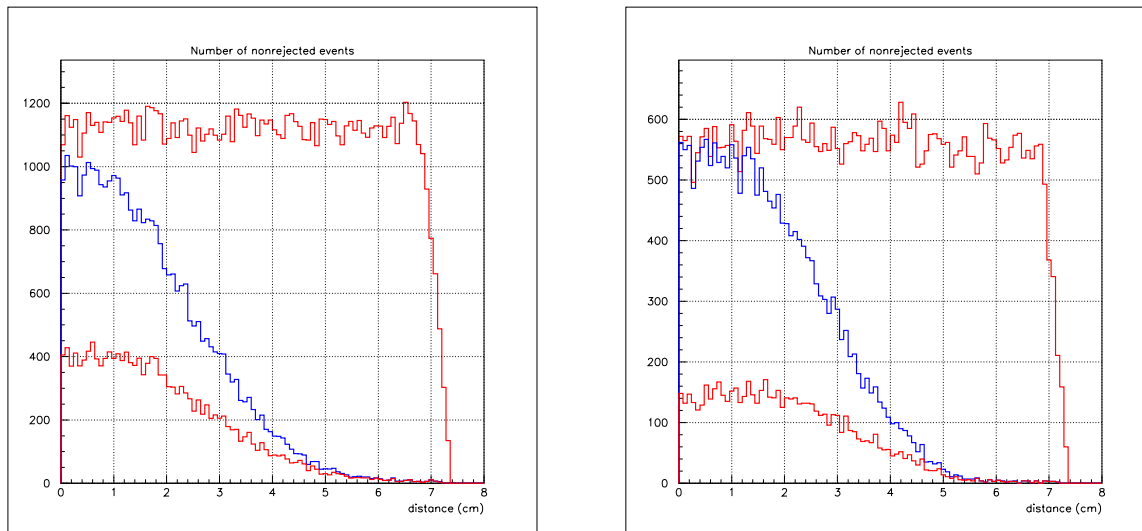


Figure 24. Results from a sample of close hit pairs as a function of the distance between the two hits with $\overline{N}_{pe}=10$ (left) and 20 (right). Original distance distribution (top curve), single electrons found after the geometrical cut (middle curve) and after the geometrical and amplitude cuts (lower curve).

The blue curve represents the amount of single electron found after the geometrical cut (clusters 10, 20 and 30). Adding the amplitude cut (set at 5% losses of single electrons) leads to the lower curves. Fig. 25 shows the resulting dhr for different settings of the amplitude cut. One sees that even with $\overline{N}_{pe}=20$ we can achieve a dhr close to 90% as required from the Monte Carlo studies of Part One. Most of the options listed in Table 8 foresee a number of photo-electrons larger than 20.

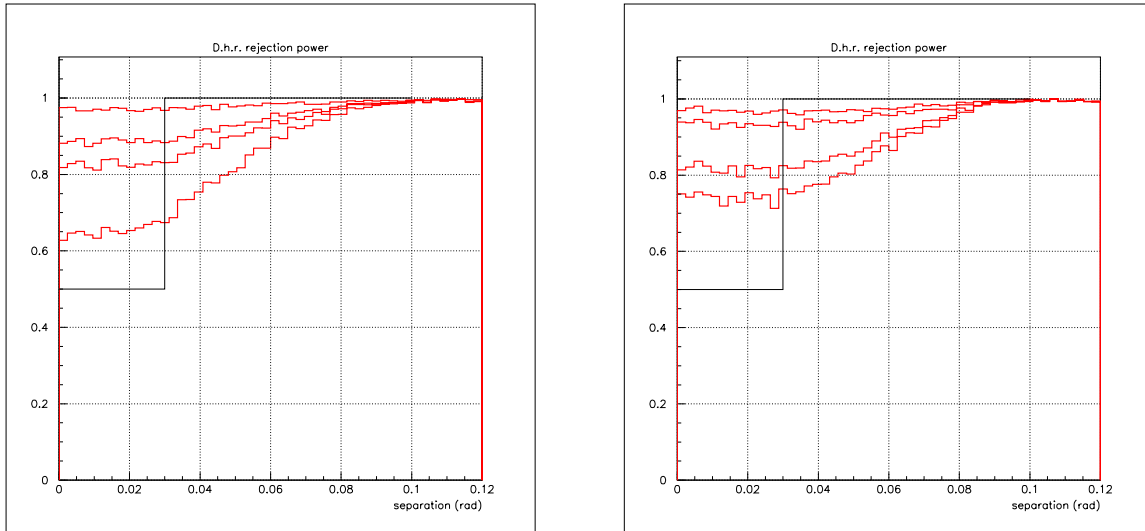


Figure 25. DHR probability as a function of the pair opening angle. The curves in the left panel are calculated for $\overline{N}_{pe} = 10$ and single electron losses of 50%(upper curve), 25%, 15% and 5%. The curves in the right panel are for $\overline{N}_{pe} = 20$ and losses of 25%(upper curve), 15%, 5% and 2%.

8.4. Residual magnetic field

In this note we assumed that the magnetic field in the volume of the HBD is fully compensated, however that might be not the real situation. It is suggested here that some residual magnetic field inside the HBD volume can be beneficial for the detector performance.

The purpose of the HBD is to detect the electrons from pairs where only one electron is detected in the PHENIX central arm, whereas the second electron is not seen by PHENIX because it has a p_T below 200MeV. It would be reasonable to require that the residual field in the HBD is such that the blob distortion for an electron with $p_T > 200\text{MeV}$ is comparable to the distortion due to the chromatic aberration (see Table 5). The second electron of the pair will then suffer a much larger distortion resulting in an elongation of the blob. That feature might be exploited for the DHR.

9. R&D PROGRAMME

Based on presently available information as described in the previous sections, we believe that an HBD can be built that fulfills the requirements for low-mass dilepton measurement in PHENIX. The first choice that emerges is a relatively simple design: an HBD with proximity focus in a windowless configuration, using CF_4 as a radiator and detector gas, with CsI solid photocathode and GEM as detector element. From the discussions presented in this note it is clear that a number of issues and critical parameters remain questionable or should be confirmed and further R&D is therefore necessary. For all these

questions, several backup options exist to solve potential problems which may arise.

The R&D necessary is both on simulations and hardware.

On the simulation front:

- We have to perform more realistic Monte Carlo studies of the expected performance including all sources of background and in particular open charm, as well as all signal sources. This can be done by embedding e^+e^- pairs generated with EXODUS into HIJING events and running them through PISA. This should allow us to assess the ultimate limit of rejection which can be achieved by the close hit cut. This work is already in progress.
- We also need to include the basic concept of the HBD in the full PHENIX Monte-Carlo in order to study and optimize its response to low-mass dileptons.

On the hardware side there are many more open questions. The most important step is a comprehensive study of CF_4 as detector gas, especially when used with GEMs and CsI . Several questions have to be addressed:

- Maximum achievable gas multiplication factor in a triple GEM configuration or in a double GEM plus MWPC operated with pure CF_4 in the presence of heavily ionizing particles.
- More study is needed on the CF_4 scintillation yield in the bandwidth of CsI sensitivity.
- Timing properties of the signals in the detector.
- Aging in pure CF_4 both of the QE of the CsI photocathode and of the GEM/MWPC elements .
- Ion feedback in GEM/MWPC configurations and possibility of gating.
- Mixtures of CF_4 with other gases, the most interesting candidate is Ne .
- One needs to optimize the GEM parameters (pitch, hole diameter and layer width). This can reduce the optical transparency on the GEM, ease the electron extraction in the holes and optimize the amplification in the first stage GEM.

Other issues not considered in this note will have to be addressed in the R&D programme:

- Optimize the magnetic field configuration.
- Study the HBD performance in the presence of some residual magnetic field.

- Readout electronics for the HBD. The gain factor in the HBD is a critical factor. Analog readout with very low noise help keeping a low enough operating voltage, minimizing the risks of breakdown and also of aging. A standard PHENIX DAQ will be desirable while testing the electronic readout.

Finally, a cosmic ray trigger will be extremely important for the realization of this R&D programme. By triggering on cosmic muons of very high energy ($\geq 4\text{GeV}$) it will be possible to study and optimize the response of the HBD to electrons. By triggering on low-energy muons the same set-up will simultaneously allow to assess and minimize the response of the HBD to hadrons.

REFERENCES

1. Y.Giomataris, G Charpak, Nucl. Insts. and Meth. A310 (1991) 589.
2. R.P.Pisani et. al., Nucl. Insts. and Meth. A400 (1997) 243-254.
3. M.Chen et.al., Nucl. Insts. and Meth. A346 (1994) 120-126.
4. B.Lasiuk, http://www.rhic.bnl.gov/qm2001/talks/tuesday_pm/2C/Lasiuk.pdf
5. A.Breskin et.al., Nucl. Insts. and Meth. A442 (2000) 58-67.
6. F.Sauli Instrumentation in high energy physics, World Scinetific, 1992. and references therein.
7. HADES experiment, Nucl. Insts. and Meth. A221 (1990) 593.
8. A.Pansky et.al., Nucl. Insts. and Meth. A354 (1995) 262-269.
9. A.Bressan, et. al., CERN-EP/98-139
10. R.Baur et.al., Nucl. Insts. and Meth. A231 (1994) p.231.
11. Buzulutskov et.al., <http://wwwhephy.oeaw.ac.at/u3w/w/wcc/www/talks/Tuesday/Buzulutskov.pdf>
12. J.Va'vra et.al., <http://wwwhephy.oeaw.ac.at/u3w/w/wcc/www/talks/Tuesday/Vavra.pdf>
13. A.Breskin <http://www.phenix.bnl.gov/WWW/run/Montauk/amos.pdf>
14. J.Va'vra et.al., SLAC-PUB-5728 May,1992
15. F.A.F.Fraga et.al., <http://wwwhephy.oeaw.ac.at/u3w/w/wcc/www/talks/Tuesday/Fraga.pdf>
16. E.g.: <http://www.bicrondirect.com/merchant/merch.jsp?&hist=-1&hist=207&hist=81>
17. P.Glässel, Nucl. Insts. and Meth. A433 (1999) 17-23.
18. S.Coutu et.al., Phys. Rev. D62, 032001(2000) 9p.